DOKUZ EYLÜL UNIVERSITY
GRADUATE SCHOOL OF NATURAL AND APPLIED SCIENCES

PRODUCTION AND DEVELOPMENT OF HIGH ELECTRICAL CONDUCTIVE AND NON-MAGNETIC ALUMINUM METAL AND ITS INDUSTRIAL APPLICATION

by
Cem ÇİLİNGİR

January, 2016
İZMİR

PRODUCTION AND DEVELOPMENT OF HIGH ELECTRICAL CONDUCTIVE AND NON-MAGNETIC ALUMINUM METAL AND ITS INDUSTRIAL APPLICATION

A Thesis Submitted to the
Graduate School of Natural and Applied Sciences of Dokuz Eylül University
In Partial Fulfillment of the Requirements for the Degree of Master of Science
in Nanoscience and Nanoengineering

by
Cem ÇİLİNGİR

January, 2016
İZMİR

M.Sc THESIS EXAMINATION RESULT FORM

We have read the thesis entitled **"PRODUCTION AND DEVELOPMENT OF HIGH ELECTRICAL CONDUCTIVE AND NON-MAGNETIC ALUMINUM METAL AND ITS INDUSTRIAL APPLICATION"** completed by **CEM ÇİLİNGİR** under supervision of **PROF. DR. ERDAL ÇELİK** and we certify that in our opinion it is fully adequate, in scope and in quality, as a thesis for the degree of Master of Science.

Prof. Dr. Erdal ÇELİK

Supervisor

Prof. Dr. Mustafa TOPARLI

(Jury Member)

Prof. Dr. Ahmet TÜRK

(Jury Member)

Prof.Dr. Ayşe OKUR
Director
Graduate School of Natural and Applied Sciences

ACKNOWLEDGEMENTS

First of all, I would like to express my deep sense of gratitude to my advisor Prof. Dr. Erdal ÇELİK for his constructive ideas, help, constant support, guidance and contributions during my MSc research. I would also like to thank Prof. Dr. Ahmet TÜRK from Celal Bayar University Material Engineering Department and Assoc. Prof. Dr. Özgül KELEŞ from Istanbul Technical University Metallurgical and Materials Enginnering Department for reviewing my work and offering valuable suggestions and sharing their visions about the content of my thesis.

I would like to thank Volt Electric Motor Company for supplying materials that I used in my study and to financial support. This research funded by Technological Research Council of Turkey (TUBITAK) between 2013 and 2015 with the project number 3130443. I also would like to thank my all colleagues in Volt Electric Motor Company especially Mustafa Hakan ÖZCOŞKUN, Bilal Volkan ŞEREFHANOĞLU, Sabri YILDIRIM, Oğuzhan TOKGÖZ and Uğur ERDOĞAN for their cooperation and friendship. I would also like to thank all the administrative and academic staff in Center for Fabrication and Application of Electronic Materials (EMUM) especially Çağlar ÖZER, Serdar YILDIRIM and Metin YURDDAŞKAL for their support and encouragement.

I wish to extend special thanks to Yıldız ÇELİK, Samet ALTUN, Murat ÖZCAN, Nihat AKDEMİR, Ahmet ERGÜL, Aytuğ GÜNER and Anıl UZUNEL for sincere assistance, support and their kind friendship at all times.

Finally, I reserve my most sincere thanks to my family for their concern, confidence and support.

Cem ÇİLİNGİR

PRODUCTION AND DEVELOPMENT OF HIGH ELECTRICAL CONDUCTIVE AND NON-MAGNETIC ALUMINUM METAL AND ITS INDUSTRIAL APPLICATION

ABSTRACT

In this research, it was aimed to be produced, improved and industrially applied high conducting and non-magnetic aluminum based materials in rotor thereby reducing the rotor conductor losses and increasing motor efficiency. In this respect, co-melting 99.7 percent aluminum metal was provided by adding seperately different ratios of aluminum boron master alloys as inoculant materials using an electric melting furnace. During the interaction of boron with impurity elements at high temperature and formation of borides, it was provided that borides came in slag. After that, it was realized that the metal eleminated magnetic behaviour and increased conductivity is casted by removing impurity elements in aluminum metal. After the casting process, this metal was subjected to heat-treatment to obtain certain textures in the structure. This treatment was provided extra high conductivity to the metal at desired directions.

With realization of this study, extra high conducting and non-magnetic materials were produced by an innovative approach without changing system and increasing cost effects compared with present state and thus efficiency of electrical engines was increased.

Keywords: Energy losses, electrical motor, rotor, rotor losses, aluminum, electrical conductivity, motor efficiency, aluminum boron, inoculation, heat treatment, texture

MANYETİK OLMAYAN YÜKSEK ELEKTRİK İLETKENLİĞE SAHİP ALÜMİNYUM METALİNİN ÜRETİMİ, GELİŞTİRİLMESİ VE ENDÜSTRİYEL UYGULAMASI

ÖZ

Bu araştırmada, elektrik motorlarındaki rotor iletken kayıplarını azaltmak ve motor verimliliğini artırmak amacıyla rotor içerisinde manyetik olmayan ve iletkenliği yüksek alüminyum esaslı malzemelerin üretimi, geliştirilmesi ve endüstriyel uygulaması hedeflenmiştir. Bu kapsamda, bir elektrikli ergitme ocağı kullanılarak yüzde 99,7 saflıkta alüminyum metali içerisinde farklı oranlarda alüminyum bor master alaşımı aşılayıcı malzeme olarak ayrı ayrı ilave edilerek birlikte ergitilmesi sağlanmıştır. Yüksek sıcaklıkta empürite elementleriyle borun etkileşime girmesi ve borürleri oluşturması sonrasında, borürlerin cürufa geçmesi sağlanmıştır. Bunun sonucunda üretilen alüminyum metalinin içerisindeki empürite elementlerin giderilmesiyle manyetikliği giderilmiş ve iletkenliği artırılmış metalin dökümü gerçekleştirilmiştir. Dökülen alüminyum metali ısıl işlem prosesine maruz bırakılarak belli yönlerde yönlenmiş malzemelerin üretimi yapılmıştır. Bu sayede alüminyum metaline ekstra iletkenlik artışı sağlanarak yüksek iletkenlik sahibi metalin üretimi gerçekleştirilmiştir.

Bu çalışmanın gerçekleşmesiyle; inovatif bir yaklaşımla sistemi bozmadan, maliyetleri artırmadan, mevcut metale göre iletkenliği yüksek ve manyetikliği giderilmiş malzemelerin elde edilmesi sağlanacak ve sonuçta elektrik motorlarının verimi artırılması sağlanmıştır.

Anahtar kelimeler: Enerji kayıpları, elektrik motoru, rotor, rotor kayıpları, alüminyum, elektrik iletkenliği, motor verimi, alüminyum bor, aşılama, ısıl işlem, tekstür

CONTENTS

Page

LIST OF FIGURES

Page

LIST OF TABLES

Page

CHAPTER ONE
INTRODUCTION

The industry have approximately 50% of energy consumption in Turkey. Also, squrriel-cage asynchronous motors use approximately 70% of this energy. In this context, energy consumption takes 97% proportion of its life cycle costs. As a result of this situation, enviromentally designs should be made for electric motors. According to analysis of electric motor losses, there are many sources of motor losses such as friction and wind losses (5%-15%), core (iron) losses (15%-25%), stator (I^2R) losses (25%-40%), rotor (I^2R) losses (15%-25%), stray load (10%-20%) (U.S. Department of Energy, 2008). Rotor losses have a part in in motor losses approximately 15%-25%, as a consequence of this reason, rotor materials should have high energy efficiency. Nowadays, commercial pure aluminum (99.7% Al) and copper (Cu) are used in squrriel-cage rotor production. Although copper have high electrical conductivity, it have high cost because of its density and high melting temperature. Aluminum has lightness, low cost, low melting temperature as well as its electrical conductivity lesser than cooper (~57 % IACS) (ASM International, 1990). Impurity elements such as Fe, Ti, Cr, V, Si, Zr, Cu, Mg and Ni decrease electrical conductivity of aluminum. In addition to this, Fe and Ni give a few magnetic properties to aluminum. In these circumstances, high losses in squrriel-cage asynchronous motors cause to decrease energy efficiency. In this case, it is aimed to minimize the energy losses in the squrriel-cage asynchronous electric motors.

In this research, it is aimed to be produced, improved and industrially applied high conducting and non-magnetic Al based materials in rotor thereby reducing the rotor conductor losses and increasing motor efficiency. In this respect, commercial pure aluminum (99.7% Al) is melted with electrical melting furnace and the melted aluminum (99.7% Al) is inoculated by Al-3B master alloy. During the interaction of boron with impurity elements at high temperature and formation of borides, it is precipiated as a intermetallic compounds out solid solution. When the borides that have high density settle at bottom of the crucible, the other borides that have low

density pass to slag and are separated into liquid metal. The borides in the liquid metal disperse as a second phases. After that, it was realized that the metal eleminated magnetic behaviour and increased conductivity is casted by removing impurity elements in Al metal. After the casting process, this metal was subjected to heat-treatment to obtain certain textures in the structure. This treatment was provided extra high conductivity to the metal at desired directions.

With realization of this study, extra high conducting and non-magnetic materials were produced by an innovative approach without changing system and increasing cost effects compared with present state and thus efficiency of squrriel-cage asynchronous electrical motors was increased. Phase analysis of this materials was observed using X-Ray Diffractometer (XRD) and its microstructure was observed using Scanning Electron Microscope and Energy Dispersive X-Ray Spectrometer (SEM/EDS). For the elemental analysis Optical Emission Spectrometer and X-Ray Photoelectron Spectrometer (XPS) were used respectively. For the analysis of electrical conductivity and magnetic properties Fischer Sigmascope SMP10 and Vibrating Sample Magnetometer (VSM) devices were used respectively.

CHAPTER TWO
THEORETICAL BACKGROUND

2.1 Asynchronous Motors

An induction or asynchronous motor operates with electromagnetic induction which is obtained by magnetic field of the stator winding of the rotor. Therefore induction motor does not need mechanical regulation, separate-excitation or self-excitation, in order to transfer energy from stator to rotor, as in universal, DC and large synchronous motors. There are two types of rotors can be used in an induction motor; wound type or squirrel-cage type.

Figure 2.1 An asynchronous motor (incompleted).

Figure 2.2 Three phase asynchronous motor parts: (1) v ring, (2) end shield de, (3) compensation ring, (4) shaft, (5) de-nde bearing, (6) rotor, (7) terminal box cover, (8) terminal box cover seal, (9) terminal box, (10) cable gland, (11) name plate, (12) housing, (13) foot, (14) stator, (15) end shield nde, (16) fan. (Volt Electric Motors Catalog, 2013).

Three-phase squirrel-cage induction motors are solid, stable and economical, thus they are oftenly used in industrial drives. Single-phase induction motors are fragile and they are not so powerful, therefore they widely used for smaller loads, such as fans. Induction motors are used in fixed-speed services, but they are increasly being used with variable-frequency drives (VFDs) in variable-speed service. When VFDs are being used efficiently, energy savings opportunities for existing and probable solutions in variable-torque centrifugal fans, pumps and compressors. Squirrel cage induction motors are very widely used in both fixed-speed and variable-frequency drive (VFD) applications.

2.1.1 Squirrel-Cage Rotors

A squirrel cage rotor includes a cage, lamination sheets provided with a plurality of slots, and short circuit rings arranged at the axial ends of said lamination sheets and connected by short circuit rods disposed within said slots. In one aspect, said lamination sheets comprise sheets made of an amorphous magnetic material, especially of an amorphous metal with high saturation magnetization. In another aspect, said slots are formed with a convex base portion. In a further aspect, said short circuit rings are made of a metal matrix composite material with high electrical conductivity, preferably of a fiber reinforced aluminum matrix composite material.

Figure 2.3 Squirrel-cage rotors.

2.1.2 Structure

The motor rotor shape is a cylinder mounted on a shaft. Internally it contains longitudinal conductive bars (usually made of aluminum or copper) set into grooves and connected at both ends by shorting rings forming a cage-like shape. The name is derived from the similarity between this rings-and-bars winding and a squirrel cage.

The solid core of the rotor is built with stacks of electrical steel laminations. Figure 3 shows one of many laminations used. The rotor has a smaller number of slots than the stator and must be a non-integer multiple of stator slots so as to prevent magnetic interlocking of rotor and stator teeth at the starting instant (Gupta, 2010).

The rotor bars may be made either of copper or aluminum. A very common structure uses die cast aluminum poured into the rotor after the laminations are stacked. Some larger motors have aluminum or copper bars which are welded or brazed to end-rings. Since the voltage developed in the squirrel cage winding is very low, no intentional insulation layer is present between the bars and the rotor steel (Slemon, 1966).

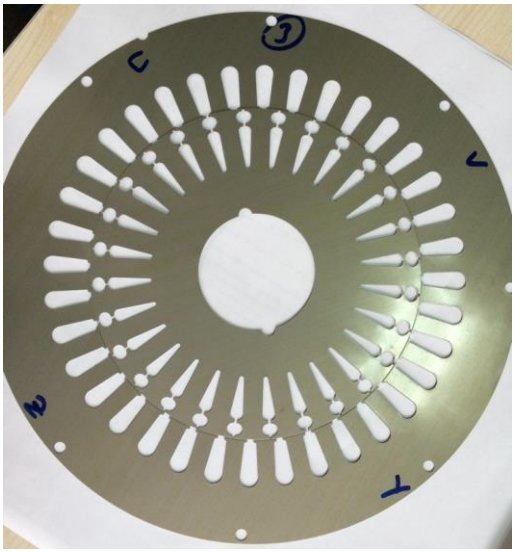

Figure 2.4 Rotor and stator lamination.

2.1.3 Theory

The field windings in the stator of an induction motor set up a rotating magnetic field through the rotor. The relative motion between this field and the rotor induces electric current in the conductive bars. In turn these currents lengthwise in the conductors react with the magnetic field of the motor to produce force acting at a tangent orthogonal to the rotor, resulting in torque to turn the shaft. In effect the rotor is carried around with the magnetic field but at a slightly slower rate of rotation. The difference in speed is called slip and increases with load (Slemon, 1966).

The conductors are often skewed slightly along the length of the rotor to reduce noise and smooth out torque fluctuations that might result at some speeds due to interactions with the pole pieces of the stator. The number of bars on the squirrel cage determines to what extent the induced currents are fed back to the stator coils and hence the current through them. The constructions that offer the least feedback employ prime numbers of bars.

The stator consists of a core of thin, insulated laminations made of silicon steel. These laminations are stacked and compressed and held in place by either banding or welding beads along the length of the stack. The Stator has slots into which copper wire is inserted. Leads are connected to the windings and brought out to a junction box to connect to three-phase power (Slemon, 1966).

The rotor consists of a core made of the same thin laminations of silicon steel that the stator uses, but instead of copper windings has several bars which run along its length which are connected to end rings. If the steel laminations were to be removed, these bars look like a squirrel cage, hence the name, squirrel cage induction motor.

The same basic design is used for both single-phase and three-phase motors over a wide range of sizes. Rotors for three-phase will have variations in the depth and shape of bars to suit the design classification. Generally, thick bars have good torque and are efficient at low slip, since they present lower resistance to the EMF. As the

slip increases, skin effect starts to reduce the effective depth and increases the resistance, resulting in reduced efficiency but still maintaining torque (Slemon, 1966).

The shape and depth of the rotor bars can be used to vary the speed-torque characteristics of the induction motor. At standstill, the revolving magnetic field passes the rotor bars at a high rate, inducing line-frequency current into the rotor bars. Due to the skin effect, the induced current tends to flow at the outer edge of the winding. As the motor accelerates, the slip frequency decreases and induced current flows at greater depths in the winding. By tapering the profile of the rotor bars to vary their resistance at different depths, or by constructing a double squirrel cage, the motor can be arranged to produce more or less torque at standstill and near its synchronous speed (Slemon, 1966).

2.1.4 Efficiency Classification in Low-Voltage Motors According to IEC60034-30

IEC/EN 60034-34 has been published by IEC in October of 2008. Its purpose is to eliminate the numerous different energy standards used for cage-induction motors and to create a single description for low-voltage motors efficiencies to be used globally.

These efficiency classes are:

- Premium efficiency IE3
- High efficiency IE2
- Standard efficiency IE1

IE4 class was defined in IEC 60034-30:2008 for asynchronous and synchronous motors. 15% more efficiency was aimed with respect to IE3 motors. Innovations in cage rotor designs and material technology were requested for providing IE4 efficiency. During a review of standards, this application could be added to the system at a later time.

It has a wider coverage compared to the previous standard. The standard covers most kinds of motors (i.e. general purpose standard motors, motors designed for explosive areas, marine motors and motors with reducers and brakes) (Volt Electric Motors, 2015).

Properties of IE2 motors covered by this standard are:

- Three-phase, single-speed asynchronous motors; 50 Hz and 60 Hz
- Motors with power between 0.75kW and 375kW
- 2, 4 and 6-pole motors
- Motors with rated voltage up to 1000V
- Operation type S1 and operation period 80% and over S3
- Motors operating directly with delta connection

Following motors are excluded from standard are:

- Motors used with speed control devices
- Motors that cannot be tested without the appliances they are used for (i.e. pumps, fans and compressors)

Efficiency classes defined in IEC 60034-30 standard have entered into force in 2008 by IEC. Comparable efficiency levels are displayed in Figure 2.5.

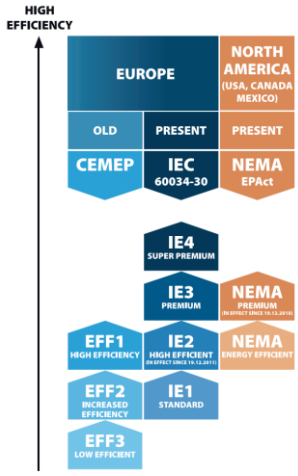

Figure 2.5 Efficiency classes defined in IEC 60034-30 standard and their comparable efficiency levels (Volt Electric Motors, 2015).

2.2 Electrical Resistivity of Metals

As mentioned previously, most metals are extremely good conductors of electricity; room-temperature conductivities for several of the more common metals are contained in Table 2.1 (Callister & Rethwisch, 2010).

Table 2.1 Room-temperature electrical conductivities for nine common metals and alloys (Callister & Rethwisch, 2010).

Metal	**Electrical Conductivity [$(\Omega m)^{-1}$]**
Silver	6.8×10^7
Copper	6.0×10^7
Gold	4.3×10^7
Aluminum	3.8×10^7
Brass (70Cu-30Zn)	1.6×10^7
Iron	1.0×10^7
Platinum	0.94×10^7
Plain carbon steel	0.6×10^7
Stainless steel	0.2×10^7

At this point it is convenient to discuss conduction in metals in terms of the resistivity, the reciprocal of conductivity; the reason for this switch in topic should become apparent in the ensuing discussion (Callister & Rethwisch, 2010).

Since crystalline defects serve as scattering centers for conduction electrons in metals, increasing their number raises the resistivity (or lowers the conductivity). The concentration of these imperfections depends on temperature, composition, and the degree of cold work of a metal specimen.

In fact, it has been observed experimentally that the total resistivity of a metal is the sum of the contributions from thermal vibrations, impurities, and plastic deformation; that is, the scattering mechanisms act independently of one another. This may be represented in mathematical form as follows (Callister & Rethwisch, 2010):

$$\rho_{total} = \rho_t + \rho_i + \rho_d \tag{2.1}$$

in which ρ_t, ρ_i and ρ_d represent the individual thermal, impurity, and deformation resistivity contributions, respectively. Equation 2.1 is sometimes known as Matthiessen's rule. The influence of each r variable on the total resistivity is demonstrated in Figure 2.6 a plot of resistivity versus temperature for copper and several copper–nickel alloys in annealed and deformed states. The additive nature of the individual resistivity contributions is demonstrated at -100°C (Callister & Rethwisch, 2010).

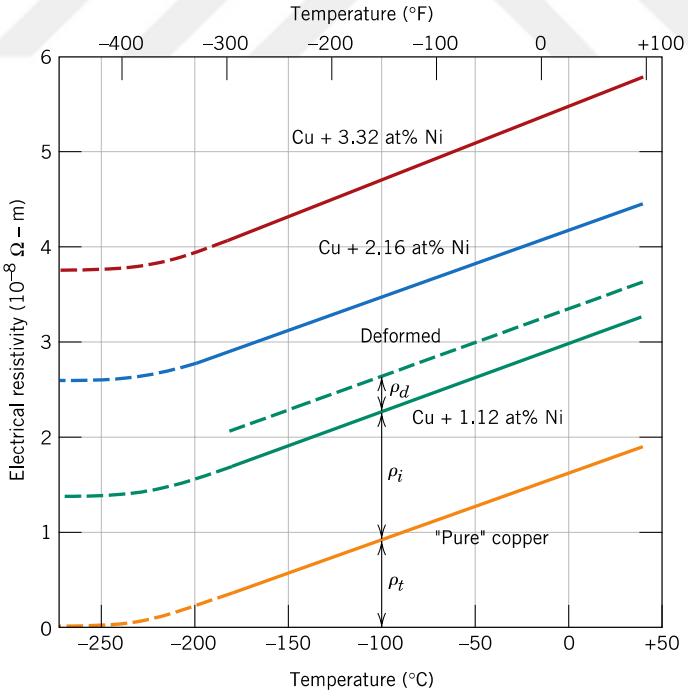

Figure 2.6 The electrical resistivity versus temperature for copper and three copper-nickel alloys, one of which has been deformed. Thermal, impurity and deformation contributions to the resistivity are indicated at -100°C (Callister & Rethwisch, 2010).

2.2.1 Influence of Temperature

For the pure metal and all the copper–nickel alloys shown in Figure 2.6, the resistivity rises linearly with temperature above about -200°C. Thus,

$$\rho_t = \rho_0 + \alpha T \tag{2.2}$$

where ρ_0 and a are constants for each particular metal. This dependence of the thermal resistivity component on temperature is due to the increase with temperature in thermal vibrations and other lattice irregularities (e.g., vacancies), which serve as electron-scattering centers (Callister & Rethwisch, 2010).

2.2.2 Influence of Impurities

For additions of a single impurity that forms a solid solution, the impurity resistivity r_i is related to the impurity concentration c_i in terms of the atom fraction (at%/100) as follows (Callister & Rethwisch, 2010):

$$\rho_i = Ac_i(1 - c_i) \tag{2.3}$$

where A is a composition-independent constant that is a function of both the impurity and host metals. The influence of nickel impurity additions on the room-temperature resistivity of copper is demonstrated in Figure 2.7, up to 50 wt% Ni; over this composition range nickel is completely soluble in copper. Again, nickel atoms in copper act as scattering centers and increasing the concentration of nickel in copper results in an enhancement of resistivity (Callister & Rethwisch, 2010).

For a two-phase alloy consisting of a and b phases, a rule-of-mixtures expression may be utilized to approximate the resistivity as follows:

$$\rho_i = \rho_\alpha V_\alpha + \rho_\beta V_\beta \tag{2.4}$$

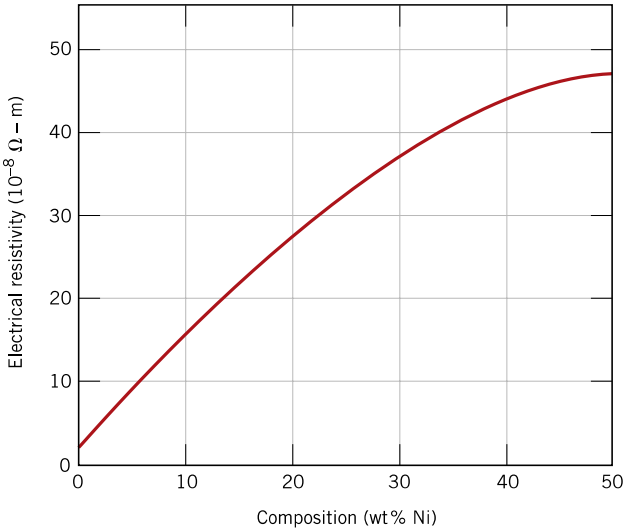

Figure 2.7 Room-temperature electrical resistivity versus composition for copper-nickel alloys (Callister & Rethwisch, 2010).

2.2.3 Influence of Plastic Deformation

Plastic deformation also raises the electrical resistivity as a result of increased num- bers of electron-scattering dislocations. The effect of deformation on resistivity is also represented in Figure 2.6. Furthermore, its influence is much weaker than that of increasing temperature or the presence of impurities (Callister & Rethwisch, 2010).

2.3 Magnetism

Magnetism is the phenomenon which materials assert an attractive or repulsive force or influence on other materials. Many of our modern technological devices rely on magnetism and magnetic materials; these include electrical power generators and transformers, electric motors, radio, television, telephones, computers, and components of sound and video reproduction systems. To better understanding magnetic materials firstly the magnetic terms and origins of magnetism should be defined (Callister & Rethwisch, 2010).

2.3.1 Origins of Magnetism

Magnetic forces are generated by moving electrically charged particles. Many times it is convenient to think of magnetic forces in terms of fields. Imaginary lines of force may be drawn to indicate the direction of the force at positions in the vicinity of the field source. The magnetic field distributions as indicated by lines of force are shown for a bar magnet in Figure 2.8. Magnetic dipoles are found to exist in magnetic materials, which, in some respects, are analogous to electric dipoles. Magnetic dipoles may be thought of as small bar magnets composed of north and south poles instead of positive and negative electric charges. Magnetic dipoles are influenced by magnetic fields in a manner similar to the way in which electric dipoles are affected by electric fields. Within a magnetic field, the force of the field itself exerts a torque that tends to orient the dipoles with the field (Callister & Rethwisch, 2010).

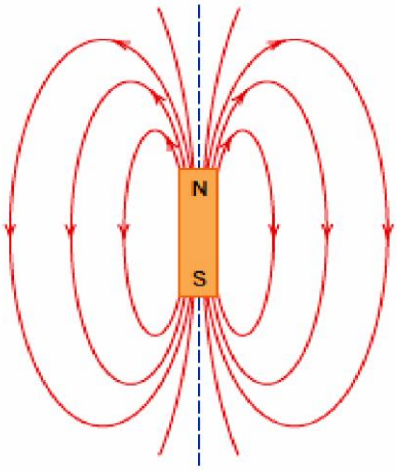

Figure 2.8 Magnetic field lines of force around a bar magnet (Callister & Rethwisch, 2010).

The externally applied magnetic field, sometimes called the magnetic field strength, is designated by H. When a magnetic field applied to a material, the response of the material is called its magnetic induction, B. The relationship between B and H is a property of the material. Magnetization of the medium is designated by M and defined as the magnetic moment per unit volume is a property of the material,

and depends on both the individual magnetic moments of the constituent ions, atoms, 16 or molecules, and on how these dipole moments interact with each other. In SI units the relationship between B, H, and M is;

$$B = \mu_0(H + M) \tag{2.5}$$

where μ_0 is the permeability of free space. The units of M are obviously the same as those of H (A/m), and those of 0 are weber/(A m), also known as henry/m. So the units of B are weber/m2 , or tesla (T) (Spaldin, 2010).

Several parameters may be used to describe the magnetic properties of solids. One of these is the ratio of the permeability in a material to the permeability in a vacuum or

$$\mu_r = \frac{\mu}{\mu_0} \tag{2.6}$$

where μr is called the relative permeability, which is unitless. The permeability or relative permeability of a material is a measure of the degree to which the material can be magnetized, or the ease with which a B field can be induced in the presence of an external H field.

The magnitude of M is proportional to the applied field as follows:

$$M = \chi_m H \tag{2.7}$$

and χm is called the magnetic susceptibility, which is unitless and indicates the degree of magnetization of a material in response to an applied magnetic field. The magnetic susceptibility and the relative permeability are related as follows:

$$\chi_m = \mu_r - 1 \tag{2.8}$$

The macroscopic magnetic properties of materials are a consequence of magnetic moments associated with individual electrons. Some of these concepts are relatively complex and involve some quantum-mechanical principles beyond the scope of this discussion; consequently, simplifications have been made and some of the details omitted. Each electron in an atom has magnetic moments that originate from two sources. One is related to its orbital motion arou nd the nucleus; being a moving charge, an electron may be considered to be a small current loop, generating a very small magnetic field, and having a magnetic moment along its axis of rotation, as schematically illustrated in Figure 2.9a (Callister & Rethwisch, 2010).

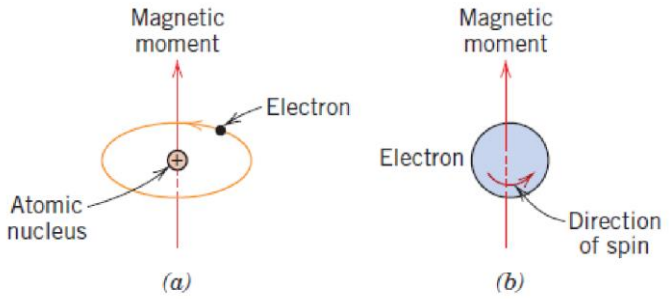

Figure 2.9 Demonstration of the magnetic moment associated with (a) an orbiting electron and (b) a spinning electron. (Callister & Rethwisch, 2010).

Each electron may also be thought of as spinning around an axis; the other magnetic moment originates from this electron spin, which is directed along the spin axis as shown in Figure 2.9b. Spin magnetic moments may be only in an "up" direction or in an antiparallel "down" direction. Thus each electron in an atom may be thought of as being a small magnet having permanent orbital and spin magnetic moments (Callister & Rethwisch, 2010).

2.3.2 Classification of Magnetic Materials

There are various types of magnetic material classified by their magnetic susceptibilities χ_m. The fundamental types have been characterized as follows: (1) diamagnetism, (2) paramagnetism, (3) ferromagnetism, (4) antiferromagnetism, (5) ferrimagnetism. All materials exhibit at least one of these types, and the behavior

depends on the response of electron and atomic magnetic dipoles to the application of an externally applied magnetic field (Moulson & Herbert, 2003).

Most materials are diamagnetic and have very small negative susceptibilities about -10^{-6}. Examples are the inert gases, hydrogen, many metals, most non-metals and many organic compounds. When a magnetic field is applied to a diamagnetic substance the electron motions are modified and a small net magnetization is induced in a sense opposing the applied field (Moulson & Herbert, 2003; Callister & Rethwisch, 2010).

Paramagnetics are those materials in which the atoms have a permanent magnetic moment arising from spinning and orbiting electrons. In the absence of an external magnetic field, the orientations of these atomic magnetic moments are random, such that a piece of material possesses no net macroscopic magnetization . An applied field tends to orient the moments and so a resultant is induced in the same sense as that of the applied field. The susceptibilities are the refore positive but again small, usually in the range 10^{-3}–10^{-6}. The atomic dipole configuration with and without a magnetic field has shown in Figure 2.10 for diamagnetic and paramagnetic materials (Callister & Rethwisch, 2010; Moulson & Herbert, 2003).

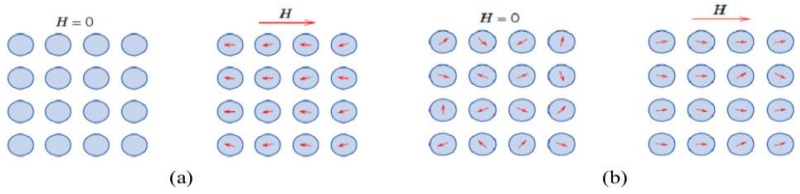

Figure 2.10 The atomic dipole configuration with and without a magnetic field, (a) for a diamagnetic material (b) for a paramagnetic material. (Callister & Rethwisch, 2010).

Certain metallic materials possess a permanent magnetic moment in the absence of an external field, and manifest very large and permanent magnetizations. These are the characteristics of ferromagnetism, and they are displayed by the transition metals iron (as BCC ferrite), cobalt, nickel, and some of the rare earth metals such as gadolinium (Gd). Magnetic susceptibilities are as high as 10^{6} possible for

ferromagnetic materials. Permanent magnetic moments in ferromagnetic materials result from atomic magnetic moments due to electron spin—uncancelled electron spins as a consequence of the electron structure (Moulson & Herbert, 2003; Callister & Rethwisch, 2010).

In antiferromagnetic materials the uncompensated electron spins associated with neighbouring cations orient themselves, below a temperature known as the Neel point, in such a way that their magnetizations neutralize one another so that the overall magnetization is zero. Metallic manganese and chromium and many transition metal oxides belong to this class. Their susceptibilities are low (about 10^{-3}) except when the temperature is close to the Neel point when the antiferromagnetic coupling breaks down and the materials become paramagnetic (Moulson & Herbert, 2003; Callister & Rethwisch, 2010).

Some ceramics also exhibit a permanent magnetization, termed ferrimagnetism. The macroscopic magnetic characteristics of ferromagnets and ferrimagnets are similar; the distinction lies in the source of the net magnetic moments. The principles of ferrimagnetism are illustrated with the cubic ferrites. These ionic materials may be represented by the chemical formula MFe_2O_4 in which M represents any one of several metallic elements (Moulson & Herbert, 2003; Callister & Rethwisch, 2010).

2.3.3 Domains and Hysteresis

Any ferromagnetic or ferrimagnetic material that is at a temperature below Tc is composed of small-volume regions in which there is a mutual alignment in the same direction of all magnetic dipole moments, as illustrated in Figure 2.11. Such a region is called a domain, and each one is magnetized to its saturation magnetizat ion. Adjacent domains are separated by domain boundaries or walls, across which the direction of magnetization gradually changes. Normally, domains are microscopic in size, and for a polycrystalline specimen, each grain may consist of more than a single domain. Thus, in a macroscopic piece of material, there will be a large number of domains, and all may have different magnetization orientations. The magnitude of

the M field for the entire solid is the vector sum of the magnetizations of all the domains, each domain contribution being weighted by its volume fraction. For an unmagnetized specimen, the appropriately weighted vector sum of the magnetizations of all the domains is zero. The formation of domains allows a ferromagnetic material to minimize its total magnetic energy, of which the exchange energy is just one component. The other main contributors to the magnetic energy are the magnetostatic energy, which is the principal driving force for domain formation, and the magnetocrystalline and magnetostrictive energies, which influence the shape and size of domains (Callister & Rethwisch, 2010).

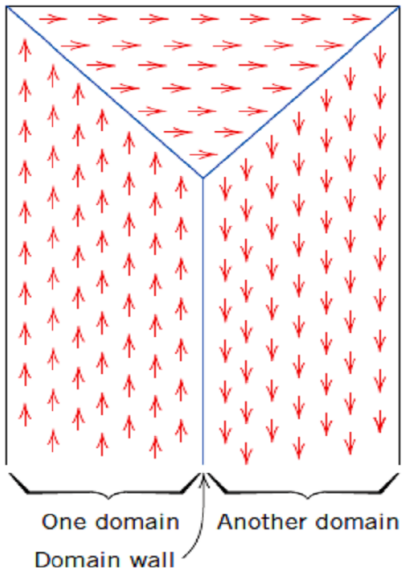

Figure 2.11 Schematic depictions of domains in a ferromagnetic or ferrimagnetic material; arrows represent atomic magnetic dipoles (Callister & Rethwisch, 2010).

As an H field is applied, the domains change shape and size by the movement of domain boundaries. Schematic domain structures are represented in the insets at several points along the B-versus-H curve in Figure 2.12. Initially, the moments of the constituent domains are randomly oriented such that there is no net B field. As the external field is applied, the domains that are oriented in directions favorable to (or nearly aligned with) the applied field grow at the expense of those that are unfavorably oriented. This process continues with increasing field strength until the macroscopic specimen becomes a single domain, which is nearly aligned with the

field. Saturation is achieved when this domain, by means of rotation, becomes oriented with the H field (Callister & Rethwisch, 2010).

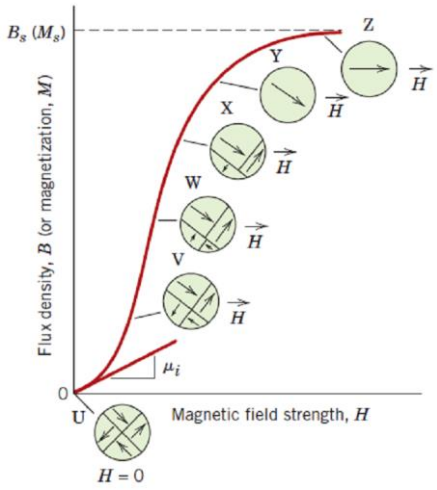

Figure 2.12 The B-versus-H behavior for a ferromagnetic or ferrimagnetic material that was initially unmagnetized. Domain configurations during several stages of magnetization are represented (Callister & Rethwisch, 2010).

2.4 Aluminum and Al-B Master Alloys

Commercial pure aluminum is often used for squrriel-cage rotor production. Rotor losses are important parameters in efficiency of electric motors. Aluminum has lightness, low cost, low melting temperature as well as its electrical conductivity lesser than cooper (~57 % IACS) (ASM International, 1990).

According to Matthiessen's Rule, the total resistivity of a metal is the sum of the contributions from thermal vibrations, impurities, and plastic deformation; that is, the scattering mechanisms act independently of one another (Callister & Rethwisch, 2010).

$$\rho_{total} = \rho_t + \rho_i + \rho_d \tag{2.9}$$

Meanings of the symbols of this formula are as follows: ρt is the electrical resistivity depending on temperature, ρi is the electrical resistivity depending on

impurity elements and ρd is the electrical resistivity depending on dislocations. Impurity elements such as Ti, Cr, V, Si, Zr, Cu, Mg, Ni and Fe decrease electrical conductivity of aluminum (Figure 2.13) (Kutner, 1981).

Al–B master alloys are widely used in the production of electrical conductive grade aluminium to remove transition metal impurities, such as titanium, vanadium, chromium and zirconium (Cooper & Kearns, 1996; Stiller & Ingenlath, 1984). These elements are brought into aluminium as impurities with bauxite or from scraps. The contents of these elements are merely higher than several tens ppm. However, as solutes, the transition elements reduce the electrical conductivity of aluminium dramatically (Willey, 1967). To overcome this problem, boron is used to precipitate these impurities by forming borides because the borides of transition metals in aluminium do not contribute to a major reduction in the electrical conductivity. Furthermore, the borides can be removed from aluminium melt by gravity settling. Due to the high stabilities of the transition metal borides compared to aluminium borides, Al–B master alloys are selected to precipitate the transition metal impurities (Cooper & Kearns, 1996).

Details on how to use the master alloys and their performance were described elsewhere (Cooper & Kearns, 1996). Al–B master alloys are also used in the in situ fabrication of aluminium matrix composites. One example is the in situ fabrication of AlB_2 fibre reinforced aluminium metal matrix composites using an Al–B master alloy (Deppisch, Liu, Shang & Economy 1997). By using an Al–5 wt.%B master alloy, an Al–AlB_2 composite reinforced with AlB_2 fibres was produced, which shows increased mechanical properties.

If these elements are transformed to boride forms with using aluminum-boron master alloys, electrical conductivity will be increased. Table 2.2 shows estimated average decrease in %IACS per wt% of impurity elements. Required quantity of the master alloys added into the furnace by using a formula which is:

$$B = \frac{M}{P}\left(\frac{Cr + Ti + V + Zr}{2}\right) \quad (2.10)$$

Meanings of the symbols of this formula are as follows: B is the total weight of the Al-B master alloy required (kg); Cr, Ti, V, Zr the concentration of impurity elements (wt.%); M the weight of aluminium to be treated (kg); and P the concentration of Al-B master alloy (wt.%) (Karabay & Uzman, 2005).

Table 2.2 Estimated average decrease in %IACS per wt% of impurity elements (Cooper, 1996)

Element	Max solubility in Al (%)	In Solution	Precipitated
Fe	0.052	29	1.2
Si	1.65	16	1.8
Ti	1.0	31	2.5
V	0.5	34	5.5
Cr	0.77	36	3.7
Zr	0.28	23	0.9

Table 2.3 Density of some compounds in the sludge (Karabay & Uzman, 2005)

Compound	Density
TiB	4.50 g/cm^3
VB_2	5.10 g/cm^3
CrB	6.15 g/cm^3
AlB_{12}	2.55 g/cm^3
AlB_2	3.19 g/cm^3

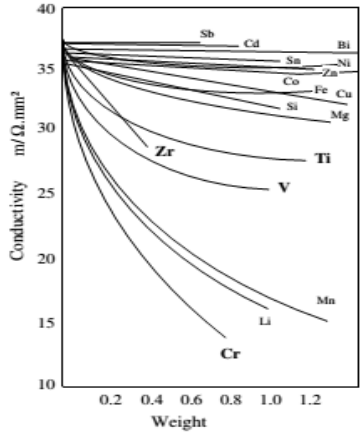

Figure 2.13 Effects of impurity elements in aluminum on electrical conductivity (Kutner, 1981).

Commercial Al–B alloys are produced via chemical reactions of KBF_4 with molten aluminium. Boron is reduced from the fluoride salt by aluminium and disperses into the alu- minium melt in the forms of aluminium borides, AlB_2 and AlB_{12}. AlB_{12} is a high temperature phase, whereas AlB_2 is stable at room temperature when the boron content is less than 44.5 wt.%, according to the Al–B phase diagram, shown in Figure 2.14. According to the phase diagram, a peritectic reaction, $L + AlB_{12} \rightarrow AlB_2$, takes place at 975 ^oC. There is a discrepancy about the peritectic temperature, which has been given in different numbers by different investigators rang- ing from 956 ^oC to 1350 ^oC (Wang, 2005).

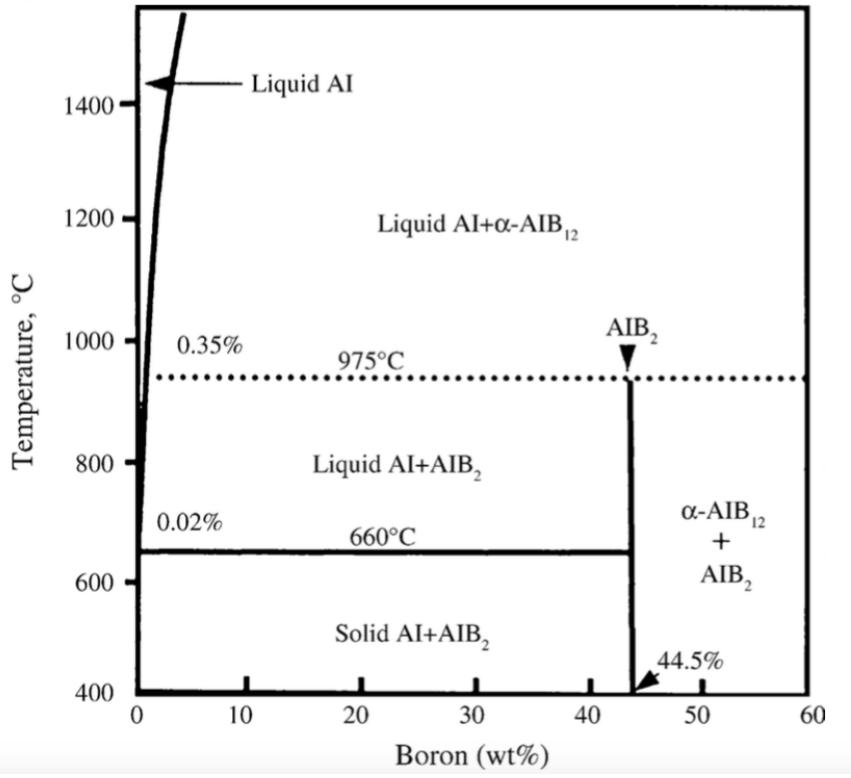

Figure 2.14 Al-rich side of Al–B phase diagram (Wang, 2005).

The XRD pattern from an Al–B bulk alloy is shown in Figure 2.15, which shows clearly the existence of the AlB_2 phase within the alloy. There are no clear AlB_{12} peaks being resolved, an indication of minor amount of AlB_{12} inside the alloy. This is in agreement with the SEM BEI image in Figure 2.16. However, it has to be noted

that the identification of AlB_{12} using the X-ray diffraction technique has been obscured by the small structure factors of boron (Wang, 2005).

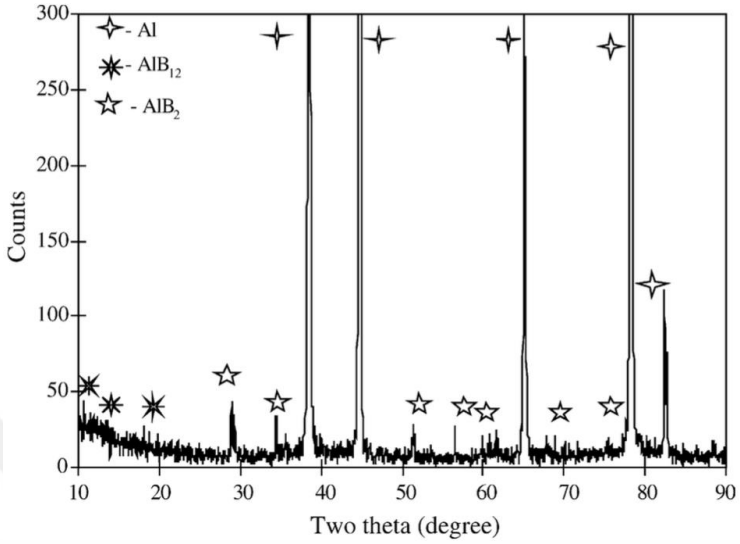

Figure 2.15 XRD pattern from an Al–B bulk alloy showing AlB_2 phase (Wang, 2005).

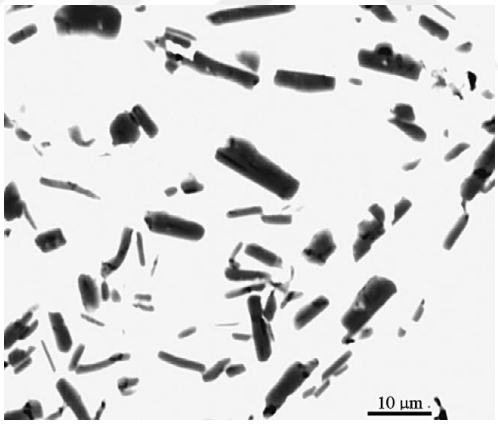

Figure 2.16 High magnification BEI image of the Al–3 wt.%B master alloys howing that boride particles contain two types of particles, small dark black particles inside large grey particles (Wang, 2005).

During cooling AlB_{12} reacts with liquid aluminium to form AlB_2. However, AlB_{12} is always detected in Al–B master alloys that have been produced via molten salt reactions at temperatures lower than the peritectic reaction temperature. The presence of AlB_{12} was also reported in Al–Ti–B master alloys that have been

produced via arc melting of aluminium and boron at 800 ^{o}C. The presence of AlB_{12} at temperatures lower than 975 ^{o}C causes confusion regarding the stabilities of the boride phases in aluminium (Zupanic, Spaic & Krizman, 1998).

AlB_2 has a hexagonal close packed (HCP) crystal structure with lattice parameters: a=0.3006nm and c=0.3252nm, whereas AlB_{12} has a tetragonal crystal structure with a=1.0161nm and b=1.4238nm. Boron and aluminium occupy alternative layers in the HCP AlB_2 crystals (Hofmann & Janiche, 1936). The melting points of AlB_2 and AlB_{12} were reported as 1655±50◦C and 2163±50◦C, respectively (Giardini, 1960). Other Al–B compounds, such as AlB_{12} and AlB_{10}, were also reported (Duschanek & Rogl, 1994).

2.4.1 Previously Researches About Aluminum Alloys

There are several studies in the literature about improving mechanical and electrical specifications of aluminum.

Sabirov, Murashkin and Valiev (2013) examined the properties of nanostructured Al alloys produced by applying plastic deformation. In these study, pure Al and its alloys are used as non-ferrus materials, so they have a key role in modern engineering. These materials can be used widely due to their corrosion resistance, high mechanical properties and low cost, in automative, aircraft and structural engineering. Different elements are added into pure Al, to decrease the size of the grains in alumnium microstructure and improve the properties of this nanostructred materials.

Kirihara, Nagata and Kimura (2002) studied to improve the thermoelectric properties of Al-based materials. Al-based quasicrystal materials which are produced by them, exposed semiconductor-like electron transportation.

Quasicrystals cause transition between semiconductor and metals, produces a high Seebeck coefficent and high electrical conductivity. This situation eases the use of

metal in high temperatures. Especially, electrical conduction is changed by a function of composition of metal. Mn, Si, Pd, Re metals are added into Al alloy to obtain that. Similarly, Smontara, et al. (2008) have studied on complex Al-Pd-TE(TE=Transition Elements) alloy systems and produced thermal isolated, high electrical conductive alloys. Conductivity is increased but, in both cases, costs are increased.

Aksöz, et al. (2010) have reported the ways to increase electrical conductivity by adding Cu element, into the alloy. In this study, it is observed that thermal and electrical conductivity are changed according to compound and temperature of alloy. It is denoted that, electrical conductivity is decreased when Cu quantity and temperature are increased.

Prabhu and Ravishankar (2003) have added Si to Al alloy with same systematical way and have examined the modification of the melting system and found a significant increase in the electrical conductivity of the material produced.

Karabay and Uzman (2005) has melted pure Al that have transition elements contained impurity level with AlB_2 and AlB_{12} inoculants. In this study was reported that in high temperatures, there was an interaction between boron and transition elements and produced boride; because of the high density of borides, they went to bottom of the crucible. In this study, it is reported that 0.013% Ti, 0.011% V and 0.006% Cr contained in commercial pure Al metal, impurity elements reduces the conductivity of the metal. AlB_2 react with transition metals and the AlB_{12} inoculant material in certain concentrations and, VB_2 and the transition to the CrB slag forming materials are provided. In addition to this study, Karabay (2006; 2008) used AlB_2 inoclulant to eliminate the precipitates which are incongruent with artifical aging of extruded Al.

Artifical aging is a additional study of increase to electrical conductivity of Al metal. Feng, Liu, Ning, Liu and Zeng (2006) added Zn, Cu, Mg and Zr in aluminum.

They reported that increase the electrical conductivity of aluminum depends on heat treatment conditions.

CHAPTER THREE
EXPERIMENTAL PROCEDURE

3.1 Purpose

The aim of this thesis is to develop high efficiency squrriel-cage asynchronous motors. The industry have approximately 50% of energy consumption in Turkey. Also, squrriel-cage asynchronous motors use approximately 70% of this energy. In this context, energy consumption takes 97% proportion of its life cycle costs. As a result of this situation enviromentally designs should be made for electrical motors. According to electric motor losses analyses, there are many sources of motor losses such as friction and windage losses (5%-15%), core (iron) losses (15%-25%), stator (I2R) losses (25%-40%), rotor (I2R) losses (15%-25%), stray load (10%-20%) (U.S. Department of Energy, 2008). Rotor losses have a part in approximately 15%-25% in motor losses, as a consequence of this reason, rotor materials should have high energy efficiency.

Nowadays, commercial pure aluminum (99.7% Al) and copper (Cu) are used in squrriel-cage rotor production. Although copper have high electrical conductivity, it have high cost because of its density and high melting temperature. Aluminum has lightness, low cost, low melting temperature as well as its electrical conductivity lesser than cooper (~57 % IACS) (ASM International, 1990). Impurity elements such as Fe, Ti, Cr, V, Si, Zr, Cu, Mg and Ni decrease electrical conductivity of aluminum. In addition to this, Fe and Ni give a few magnetic properties to aluminum. In these circumstances, high losses in squrriel-cage asynchronous motors cause to decrease energy efficiency. Within the scope of this project, it is aimed to minimize the energy losses in the squrriel-cage asynchronous electric motors.

In this research, it is aimed to be produced, improved and industrially applied high conducting and non-magnetic Al based materials in rotor thereby reducing the rotor conductor losses and increasing motor efficiency. In this respect, commercial pure aluminum (99.7% Al) is melted with electrical melting furnace and the melted

aluminum (99.7% Al) is inoculated by Al-3B inoculant material. During the interaction of boron with impurity elements at high temperature and formation of borides, it is precipiated as a intermetallic compounds in solid solution. Once the borides that have high density settle at bottom of the crucible, the other borides that have low density pass to slag and are separated into liquid metal. The borides in the liquid metal disperse as a second phases. After that, it was realized that the metal eleminated magnetic behaviour and increased conductivity is casted by removing impurity elements in Al metal. After the casting process, this metal was subjected to heat-treatment to obtain certain textures in the structure. This treatment was provided extra high conductivity to the metal at desired directions.

With realization of this study, extra high conducting and non-magnetic materials were produced by an innovative approach without changing system and increasing cost effects compared with present state and thus efficiency of squrriel-cage asynchronous electrical motors was increased. Phase analysis of these materials was observed using X-Ray Diffractometer (XRD) and its microstructure was observed using Scanning Electron Microscope and Energy Dispersive X-Ray Spectrometer (SEM/EDS). For the elemental analysis, Optical Emission Spectrometer and X-Ray Photoelectron Spectrometer (XPS) were utilized respectively. For the analysis of electrical conductivity and magnetic properties, Impedance, Fischer Sigmascope SMP10 and Vibrating Sample Magnetometer (VSM) devices were used respectively.

3.2 Materials

Aluminum metal with commercial pure (99.7% Al) was used and Al-3B master alloy which has approximately 3% boron was used as inoculant. Before die casting, Al-B master alloy as pure aluminum was used to make more pure matter. Chemical compositions of these alloys were represented in Table 3.1.

3.3 Production Techniques

Pure aluminium was melted at approximately 750-800°C in electrical melting furnace. In Al metal, there are Fe, Si, Ti, Mn, Zn, Cu, Mg and Ni as impurities and to eliminate these were added Al-3B which are inoculant matter and these metals passed to slag. Figure 3.1 shows production and characterization flow for aluminium material in details.

Table 3.1 Chemical composition of materials

Elements	**Composition (%)**	
	Pure Al	**Al-3B**
Si	0.067	0.20
Fe	0.162	0.30
Cu	0.0028	-
Mn	0.00077	-
Mg	0.00022	-
Cr	0.00062	-
Ni	0.0012	-
Zn	0.0068	-
Ti	<0.00010	-
B	<0.030	2.5-3.5
V	<0.00050	-
Zr	<0.00020	-
Al	99.70	Rem.

In the first stage, 99.7% Al melting and the molten metal is kept in the furnace for cleaning of sludge and degassing of aluminum, then sampling for analyses. In the meantime temperature of the furnace is approximately 800°C. After first stage, adding required quantity of the Al-B master alloy and stirring gently 2 minutes for homogenisation. Then, molten metal is held for the reaction and the subsiding of sludge that have more density than aluminium. At the end of two hours, steps of the first stage are carried out again. After all operations, sampling was repeated for

analyses again. After casting process, Al metal which is non-magnetic and high conductive exposes atmosphere of argon gas at tempretures between 100-500°C for different periods in electrical tube furnace to heat-treatment process so be provided extra high conductivity.

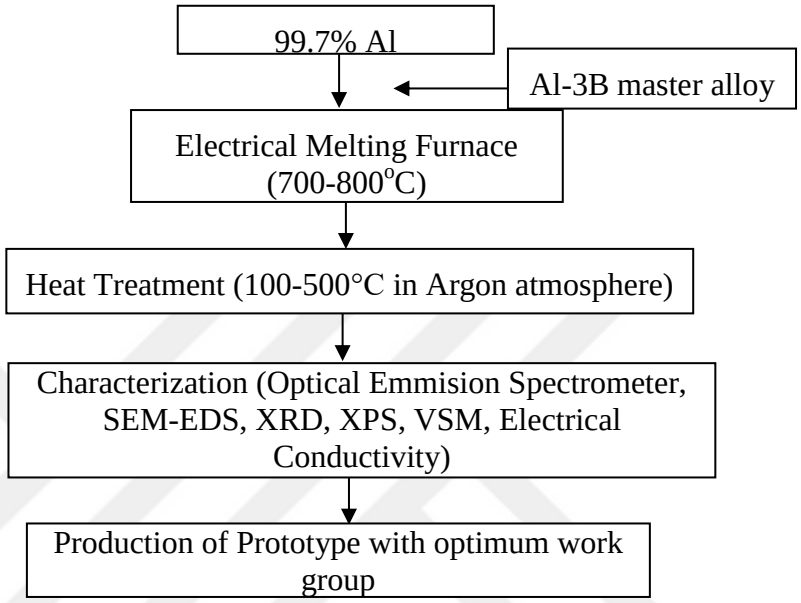

Figure 3.1 Production and characterization flow for aluminium material.

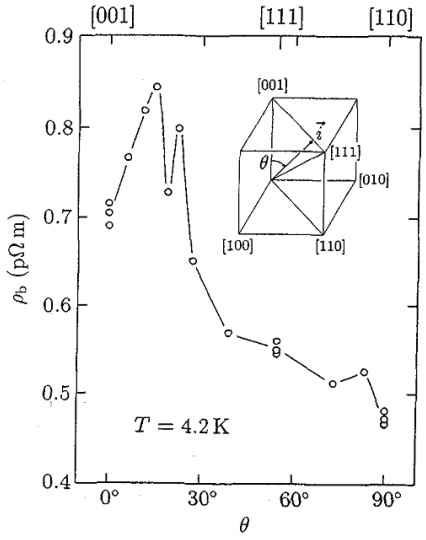

Figure 3.2 Crystallographic direction and electrical resistivity relation of 99.99% Al metal (Ueda, 1995).

As a result of the heat treatment, (110) orientation of aluminum at the plane was aimed. The plane of (110) is the highest density of free electron for FCC structure of aluminum. Therefore, electrical conductivity increase at the plane. Also material defects that occur during the production of material has been eliminated by heat treatment (Figure 3.2). After the experimental studies, choosing workgroup which has the highest efficiency to produce prototype rotor with die casting method.

3.4 Characterization

3.4.1 Spectrometer

Optical emission spectrometry involves applying electrical energy in the form of spark generated between an electrode and a metal sample, whereby the vaporized atoms are brought to a high energy state within a so called “discharge plasma”. These excited atoms and ions in the discharge plasma create a unique emission spectrum specific to each element, as shown at right. Thus, a single element generates numerous characteristic emission spectral lines (Figure 3.3). Therefore, the light generated by the discharge can be said to be a collection of the spectral lines generated by the elements in the sample. This light is split by a diffraction grating to extract the emission spectrum for the target elements. The intensity of each emission spectrum depends on the concentration of the element in the sample. Detectors (photomultiplier tubes) measure the presence or absence or presence of the spectrum extracted for each element and the intensity of the spectrum to perform qualitative and quantitative analysis of the elements.

In the broader sense, optical emission spectrometry includes ICP optical emission spectrometry, which uses an inductively coupled plasma (ICP) as the excitation source. The terms "optical emission spectrometry" and "photoelectric optical emission spectrometry," however, generally refer to optical emission spectrometry using spark discharge, direct-current arc discharge, or glow discharge for generating the excitation discharge.

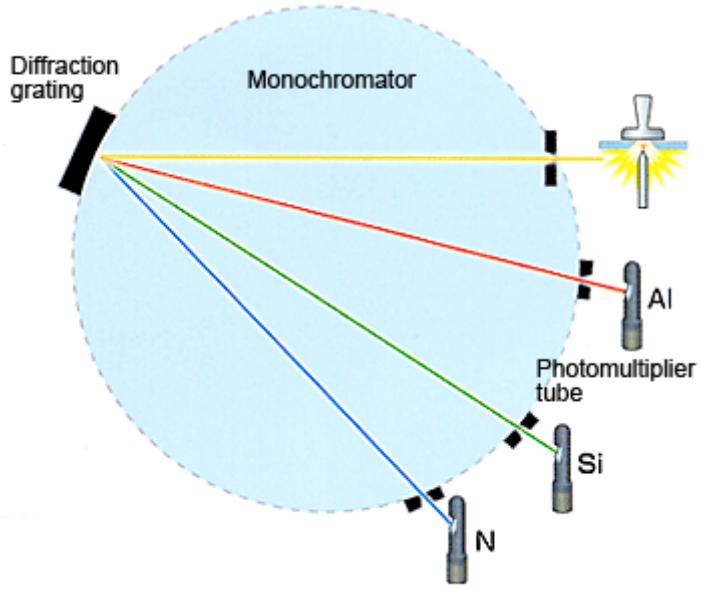

Figure 3.3 Spectrometer analysis (Shimadzu, 2015).

Shimadzu optical emission spectrometers feature Pulse Distribution Analysis (PDA) to enhance the measurement reproducibility (accuracy). This method involves statistical processing of the spark pulse-generated emission spectra obtained from spark discharges in an argon atmosphere. The optical emission spectrometer offers rapid elemental analysis of solid metal samples, making it indispensable for quality control in steel making and aluminum metallurgy processes.

3.4.2 X-Ray Diffractometer (XRD)

XRD is a powerful technique used to uniquely identify the crystalline phases present in materials and measure the structural properties (strain state, grain size, epitaxy, phase composition, preferred orientation and defect structure) of these phases. XRD is non-contact and non-destructive. The regular array of atoms in a crystalline material forms a 3D diffraction grating for waves with a wavelength around that of the distance between the atoms. When waves enter a crystal, they are scattered in all directions by the atoms. In certain directions, these waves can interfere destructively. In other directions, constructive interference will occur resulting in peaks in X-ray intensity. The diffraction pattern that results is a map of

the reciprocal lattice of the crystal and can be used to determine the structure of the crystal. Bragg's law is the basis for crystal diffraction:

$$n.\lambda=2.d.\sin\theta \qquad (3.1)$$

where n is an integer known as the order of diffraction, λ is the X-ray wavelength is the spacing between two consecutive scattering planes and θ is the angle between the atomic planes and the incident (and diffracted) X-ray beam. Figure 3.4 illustrates diffraction of x-rays by planes of atoms.

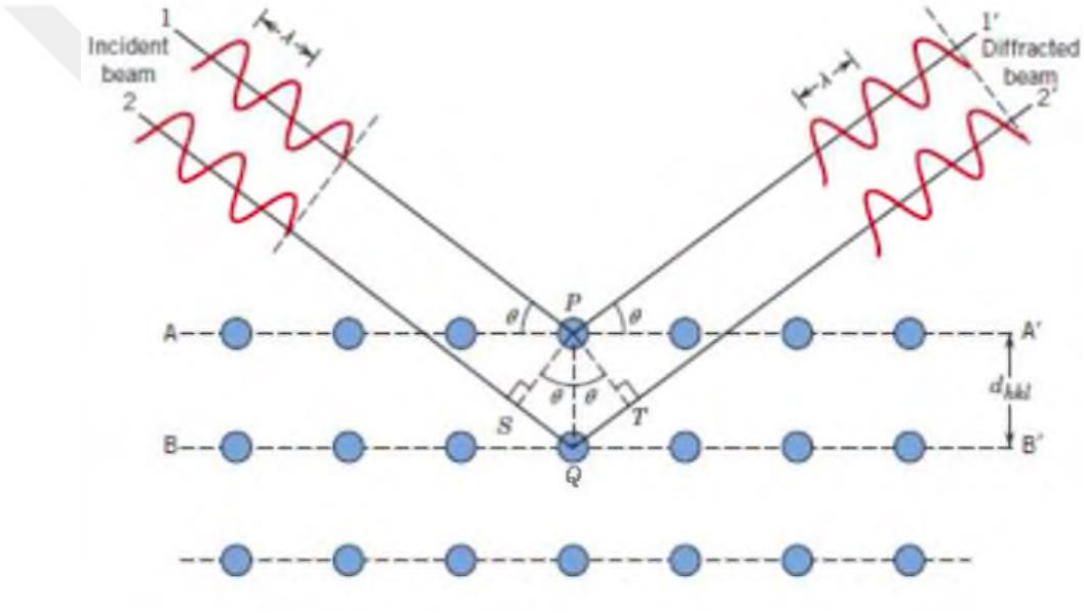

Figure 3.4 Diffraction of x-rays by planes of atoms (A-A' and B-B') (Callister, 2007).

Bragg's law is necessary but not sufficient condition for diffraction by real crystals. It specifies when diffraction will occur for unit cells having atoms positioned only at cell corners. Nonetheless, atoms situated at other sites (e.g., face and interior unit cell positions as with FCC and BCC) act as extra scattering centers, which can produce out-of-phase scattering at certain Bragg angles. The net result is the absence of some diffracted beams that, according to Bragg´s law, should be present.

X-ray diffraction (XRD) patterns of aluminum samples were determined by means of multipurpose Thermo-Scientific, ARL-K_α difractometer with a Cu K_α radiation by using multi purpose thin film attachment. Measurements were performed by applying 45 kV voltages and 44 mA current with a scanning speed of 2°/min between 30° and 90°.

3.4.3 X-ray Photoelectron Spectroscopy (XPS)

X-ray photoelectron spectroscopy (XPS) is an analyze technique which provides both elemental and chemical state information about sample material. XPS spectra are obtained by irradiating a material with a beam of X-rays while simultaneously measuring the kinetic energy and number of electrons that escape from the top 1 to 10 nm of the material being analyzed (Figure 3.5). XPS requires ultra-high vacuum (UHV) conditions and detects all elements with an atomic number (Z) of 3 (lithium) and above (Crist, 2014). In this study, elemental analyses of aluminum samples were analyzed via XPS (Thermo-Scientific Al-K_α) especially to determine substituting elements in aluminum samples.

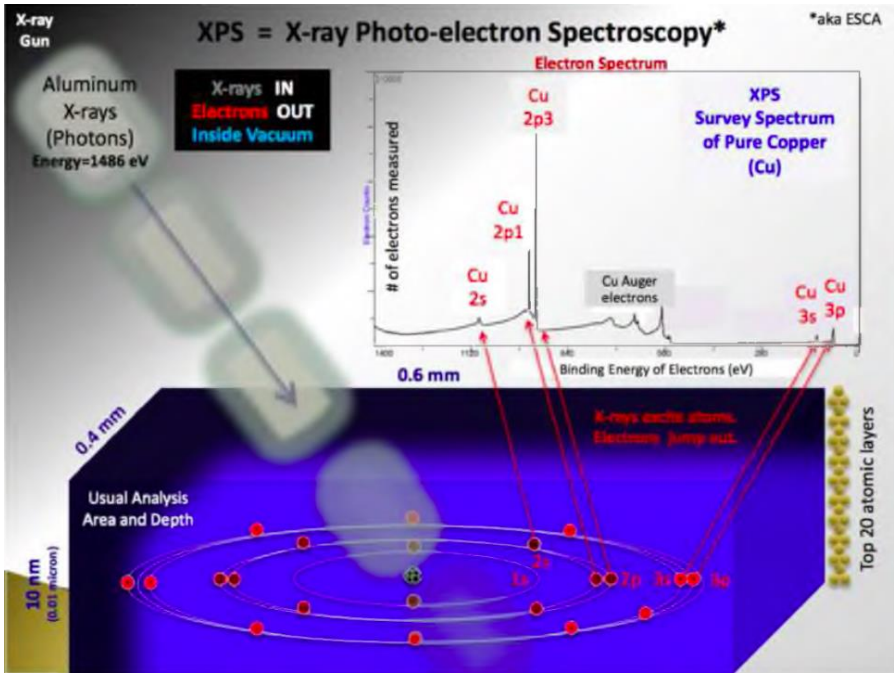

Figure 3.5 Rough schematic of XPS physics (Crist, 2011).

3.4.4 Scanning Electron Microscopy (SEM)

The Scanning Electron Microscope (SEM) is a versatile electron microscope that images a sample by scanning it with a high-energy beam of electrons in a raster scanpattern. In Typical SEM configuration, electrons are thermoionically emitted from a tungsten or LaB_6 cathode filament towards an anode. The electron beam, with a typical energy ranging from a few KeV to 30 KeV, is focused by successive lenses ina beam with a very fine spot size. When the beam introduces with the surface, differentkind of electrons can be detected. The types of signals produced by an SEM includesecondary electrons (SE), back-scattered electrons (BSE) and characteristic X-rays. Figure 3.6 illustrates the basic elements of SEM device.

The surface qualities, topographies and morphologies of aluminum samples were examined by using SEM (JEOL JSM 6060). Accelerating voltage of 15 kV was used for the SEM imaging.

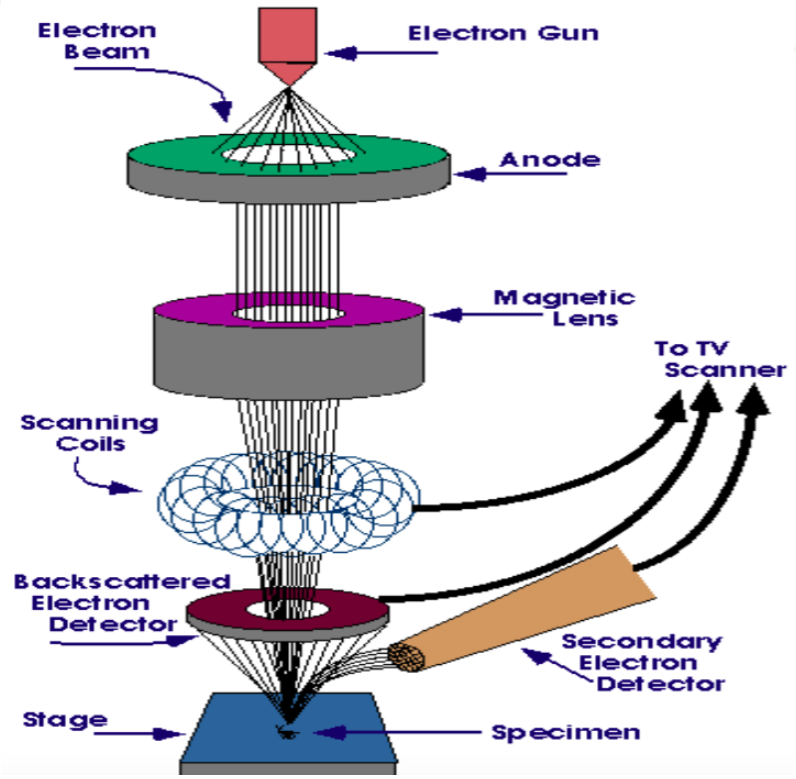

Figure 3.6 Schematic representation of SEM device (Vandaele, 2011).

3.4.5 Electrical Measurement

In this case Fischer Sigmascope® SMP 10 (Figure 3.7) was used for electrical conductivity measurements. It measures the electrical conductivity using the eddy current method according to DIN EN 2004-1 and ASTM E 1004. The phase-sensitive measurement signal evaluation enables a contact-free determination of the electrical conductivity, for example, under paint or synthetic coatings of up to 500 µm in thickness. This also minimizes the influence of surface roughness.

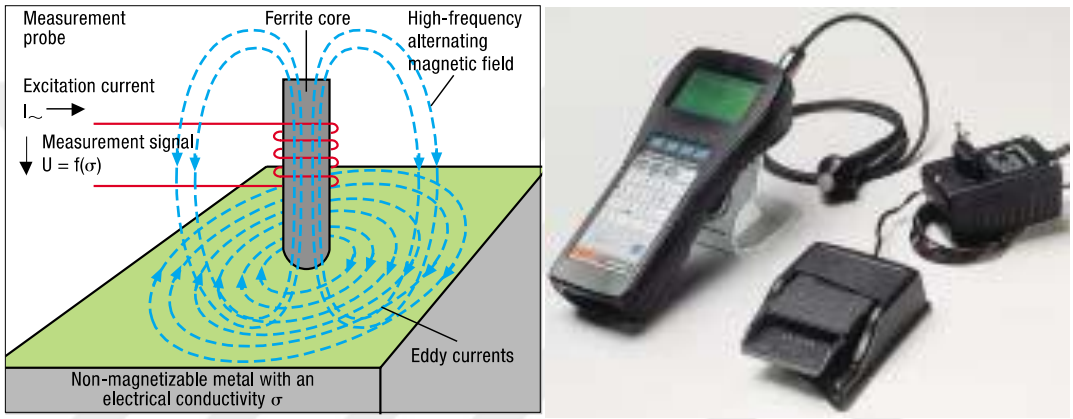

Figure 3.7 Fischer Sigmascope SMP 10 (Sigmascope, 2015)

3.4.6 Vibrating Sample Magnetometer (VSM)

A vibrating sample magnetometer (VSM) is a scientific instrument that measures magnetic properties of materials. VSM is based on Faraday's law which states that an emf will be generated in a coil when there is a change in flux linking the coil. This means that the output signal of the coil is proportional to the magnetization M but independent of the magnetic field in which the size of M is to be determined. In the VSM, the sample is subjected to a sinusoidal motion and the corresponding voltage is induced in suitably located stationary pickup coils.

The electrical output signal of these latter coils has the same frequency. Its intensity is proportional to the magnetic moment of the sample, the vibration amplitude, and the frequency. A simplified schematic representation of the VSM is

given in Figure 3.8. The sample to be measured is centered in the region between the poles of a laboratory magnet, able to generate the measuring field H_0 (Buschow & de Boer, 2004).

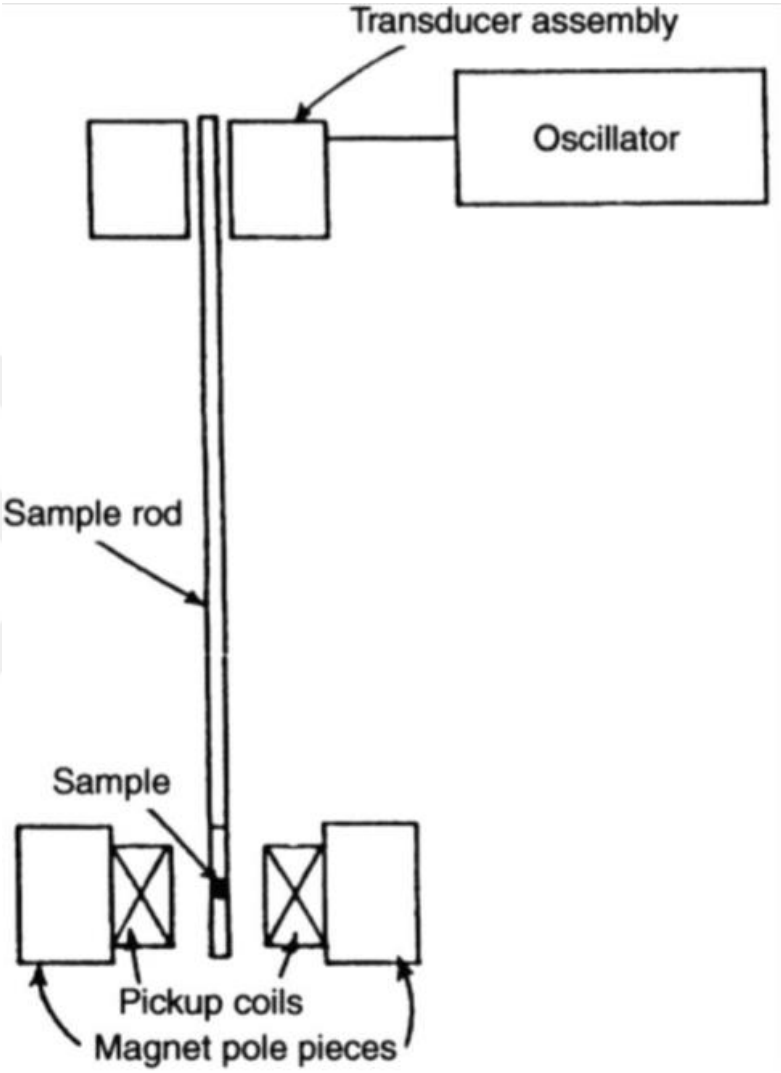

Figure 3.8 Schematic representation of Vibrating Sample Magnetometer (Buschow & de Boer, 2004).

Magnetic properties of aluminum samples were measured at room temperature by using Vibrating Sample Magnetometer (VSM Dexing Magnet Co.) with an applied field up to 11000 Oersted. Hysteresis loop, saturation magnetization (M_s), remanent magnetization (M_r) and coercivity (H_c) of aluminum samples were determined with VSM analysis.

3.5 Production of Prototype Motors and Performance Tests

After the experimental studies, choosing workgroup which has the highest efficiency to produce prototype rotor with die casting method. The efficiency of a motor is defined as the ratio of output (mechanical) power to input (electrical) power. It can be measured or determined directly or indirectly. Direct measurement involves measuring the input power on the basis of the voltage and current supplied, and the output power based on the rotational speed and torque. Indirect measurement involves measuring the input power and calculating the output power on the basis of the losses within the motor.

Motor losses can be split into five major areas (Figure 3.9) such as (1) copper losses, (2) iron losses, (3) rotor losses, (4) friction and windage losses and (5) additional load losses (PLL). Of these, the first four types of loss can be determined from input power, voltage, current, rotational speed and torque. Additional load losses (PLL) are much more difficult to determine, IEC/EN 60034-2-1 therefore specifies different methods of determining PLL which involve low, medium or high uncertainty. IEC60034-30 stipulates, however, that for motors in efficiency classes IE2 and IE3 only low uncertainty methods are acceptable. This requirement is met by the determination of PLL from residual losses measured.

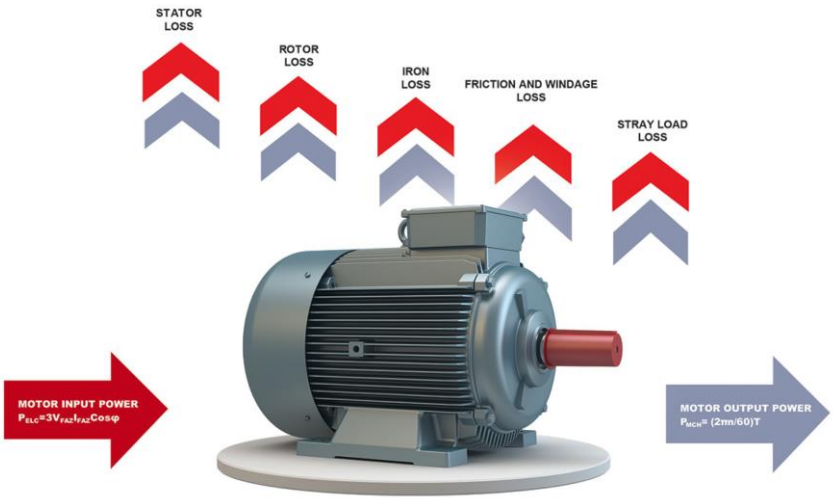

Figure 3.9 Asynchronous motor losses (Volt Electric Motors Company, 2015)

CHAPTER FOUR
RESULTS AND DISCUSSION

4.1 Spectral Analysis

Elemental analyses of all aluminum samples were determined with the help of optical emission spectrometer. The optical emission spectrometer analysis of all aluminum samples are represented in Table 4.1. In analysis, the obtained results show that after the inoculation prosess the purity of aluminum samples are increased.

Table 4.1 Chemical composition of pure and inoculated Al

Elements	**Composition (%)**	
	Pure Al	**Inoculated Al**
Si	0.067	0.057
Fe	0.162	0.131
Cu	0.0028	0.0033
Mn	0.00077	0.0012
Mg	0.00022	<0.00010
Cr	0.00062	0.00053
Ni	0.0012	0.0012
Zn	0.0068	0.0075
Ti	<0.00010	<0.00010
B	<0.030	0.029
V	<0.00050	<0.00050
Zr	<0.00020	<0.00020
Al	99.70	99.75

4.2 Phase Analysis

XRD patterns of pure Al with planes were represented in Figure 4.1 respectively. The aim of this work increase the peak of (110) plane which 65.18^{o}. The plane of (110) is the highest density of free electron for FCC structure of aluminum.

All samples were produced preparing techniques and heat treated at 100-500°C as explained in Chapter Three. The XRD patterns of heat treated at 300°C, 400°C and 500°C for 2 hours inoculated aluminum samples were compared with each others for texturing.

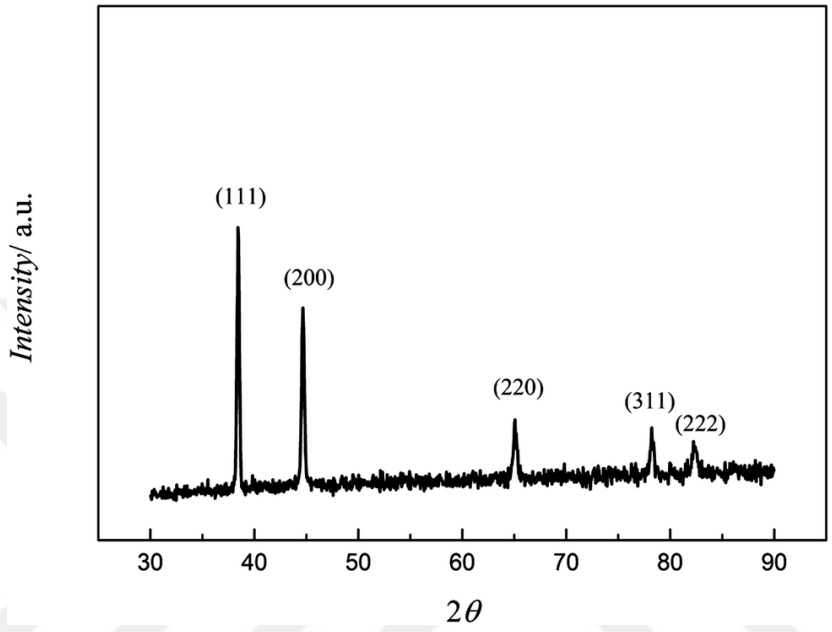

Figure 4.1 XRD pattern of the aluminum (Giridhar, 2014).

As we see in the Figure 4.2, 400-120 min sample have the highest peak in 65.18^{o}. The same sample also yielded the highest results in the conductivity results. Valance electrons of (110) plane in FCC structures have higher density than other planes, so texture on these planes causes higher electrical conductivity.

4.3 XPS Analysis

Elemental analyses of all aluminum samples were determined with the help of XPS. The XPS analysis of inoculated aluminum are represented in Figure 4.3. In analysis results the presence of B, Al, O and C elements were detected in inoculated aluminum samples. Most likely pollution of samples cause the presence of C element because XPS is a very sensitive device and presence of C element can mostly ignore.

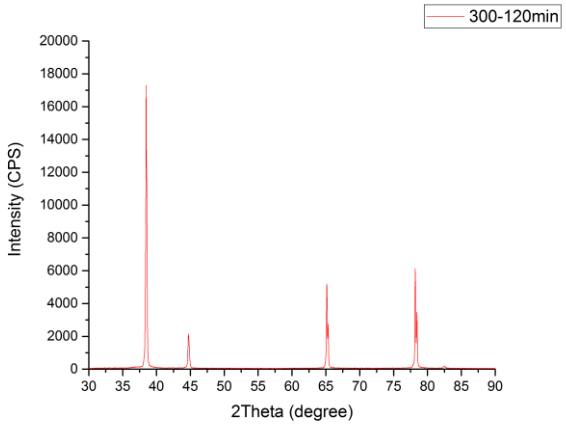

300°C-2 hours		
Peak (%)	2Θ	Intensity (cps)
100	38,43	17172.88
12.04	44,83	2068.46
30.36	**65.18**	**5215.21**
35.03	78.3	6016.69
1.07	82.34	185.16

(a)

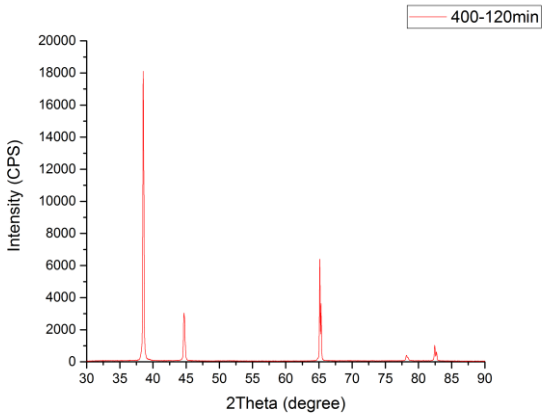

400°C-2 hours		
Peak (%)	2Θ	Intensity (cps)
100	38,43	18042.71
16.40	44,83	2959.55
35.22	**65.18**	**6355.93**
2.22	78.3	400.63
5.51	82.34	995.33

(b)

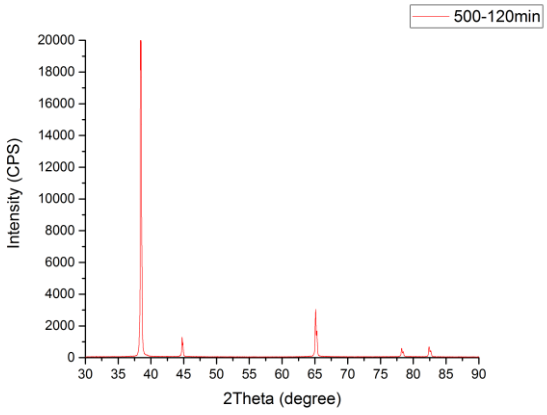

500°C-2 hours		
Peak (%)	2Θ	Intensity (cps)
100	38,43	19977.36
6.23	44,83	1245.04
15.19	**65.18**	**2835.31**
2.97	78.3	593.57
3.43	82.34	685.27

(c)

Figure 4.2 XRD analysis results of samples after heat treatment (a) at 300°C-2 hours, (b) 400°C-2 hours and (c) 500°C-2 hours.

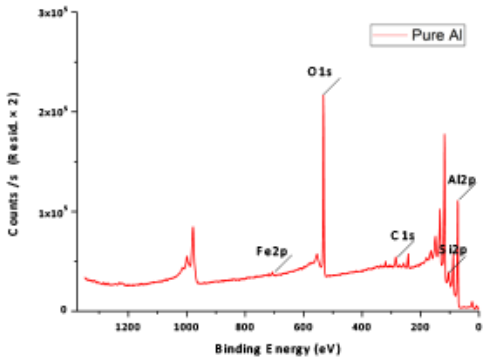

Name	*Peak BE*	*FWHM eV*	*Area (P) CPS.eV*	*At. %*
Al2p	72.87	2.682	324469.11	49.53
O1s	531.87	3.176	653262.68	23.08
C1s	284.73	3.519	47201.62	4.26
Fe2p	707.14	3.449	15795.70	0.11
Si2p	103.56	3.571	55787.35	5.66
P2p	133.40	3.501	218077.05	15.36
S2p	164.74	3.515	39266.37	2.00

(a)

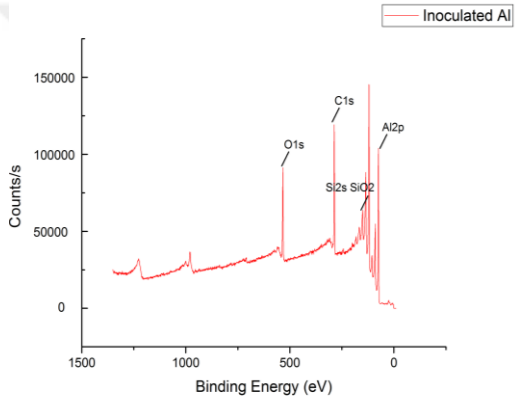

Name	*Peak BE*	*FWHM eV*	*Area (P) CPS.eV*	*At. %*
Al2p	74.61	2.227	215898.55	27.99
C1s	286.68	2.693	254540.97	15.40
O1s	533.82	2.871	200626.87	16.18
Si2s SiO2	151.05	3.451	87912.02	5.22
Al2s	119.75	2.683	373386.24	32.75
B1s	182.96	3.452	20751.07	2.46

(b)

Figure 4.3 XPS analysis and elemental ID and quantification samples (a) pure Al and (b) inoculated Al.

4.4 SEM Analysis

In order to examine the microstructure and particle sizes of intermetallics of aluminum samples, SEM images at different magnifications were taken. SEM images of Al-3B master alloy, pure aluminum and inoculated aluminum samples were represented in Figures 4.4 - 4.11.

4.4.1 Al-3B Master Alloy

SEM analysis of Al-3B master alloy is showed that the boride particules are dispersed in aluminum matrix (Figure 4.4). According to EDS Analysis this particules have AlB_{12} intermetallics (Figure 4.5).

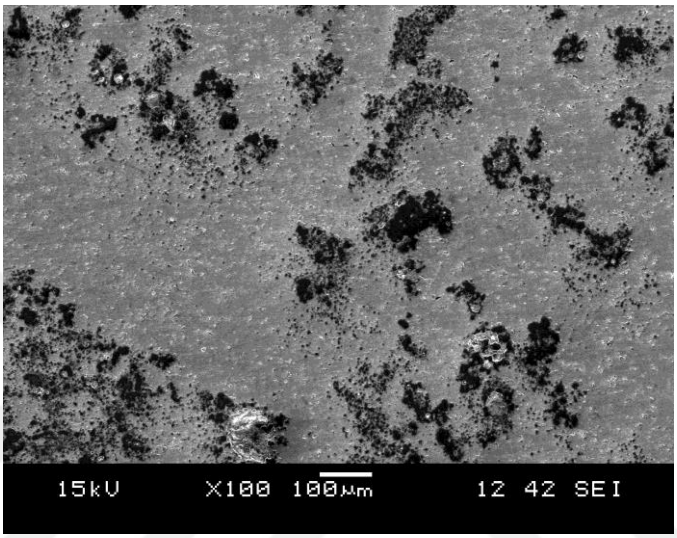

(a)

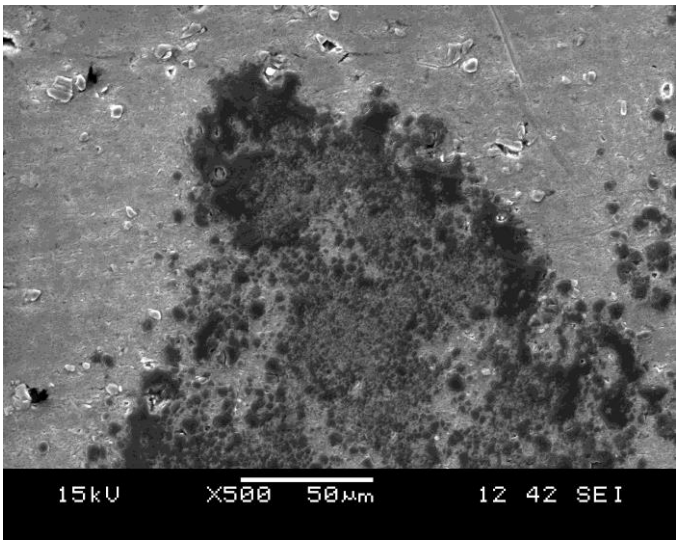

(b)

Figure 4.4 SEM images of Al-3B master alloy (a) x100 and (b) x500 magnifications.

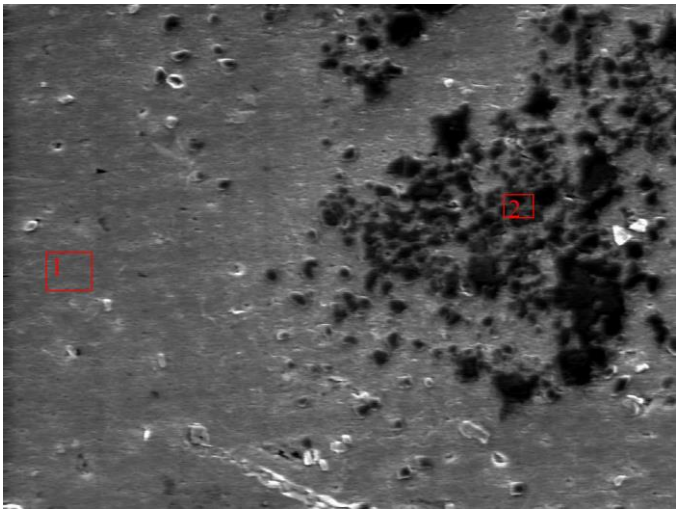

(a)

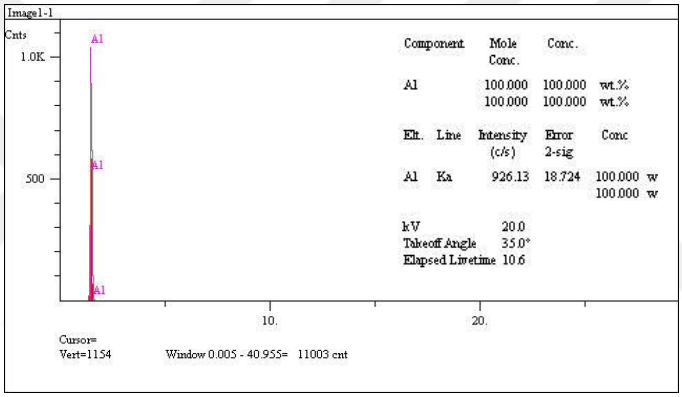

(b)

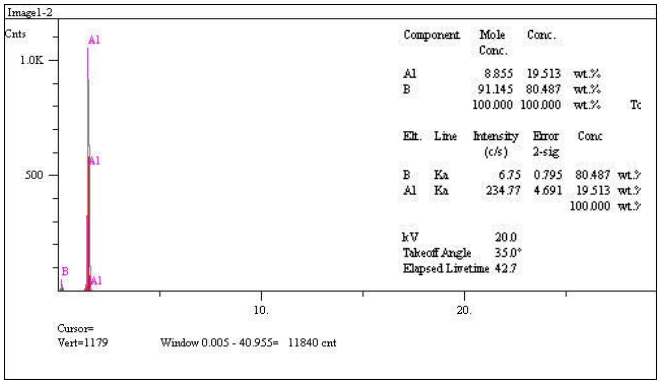

(c)

Figure 4.5 EDS analysis of Al-3B master alloy (a) image at x750 magnification, (b) matrix analysis and (c) the boride particules analysis.

4.4.2 Before and After Inoculation

SEM analysis pure and inoculated aluminum were represented in Figures 4.6 and 4.7. Their EDS analyses were represented in Figures 4.8, 4.9, 4.10 and 4.11.

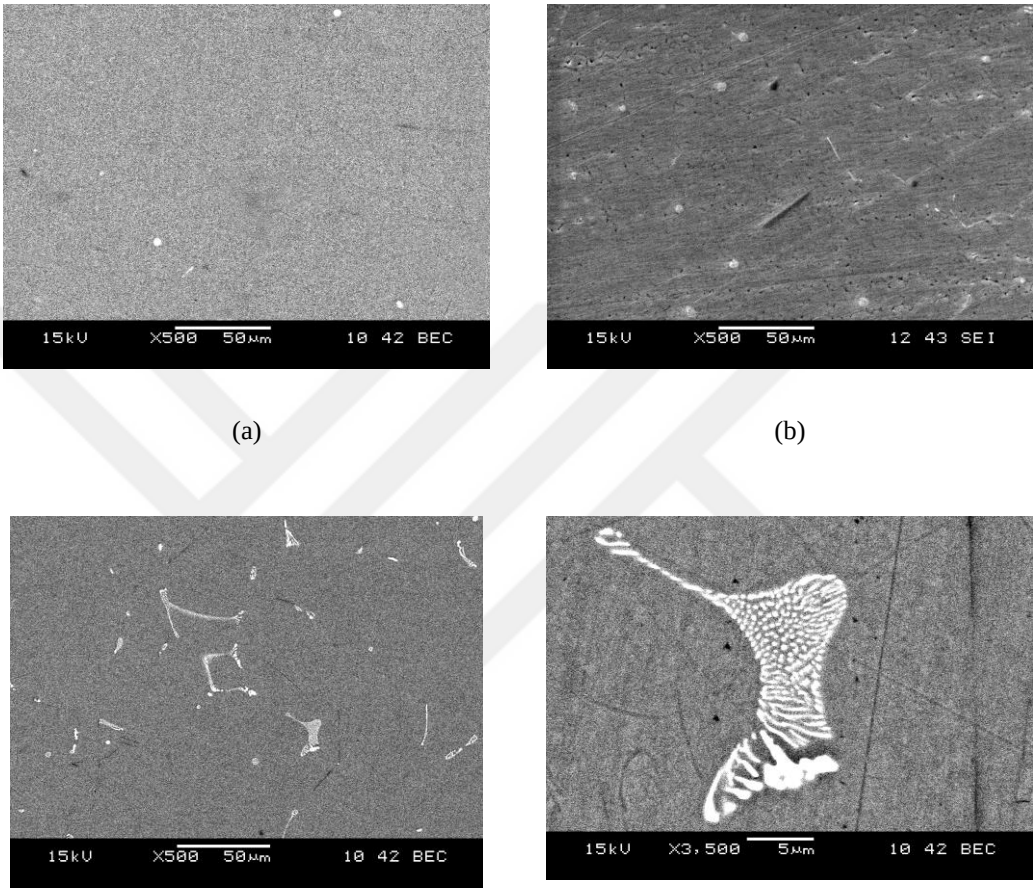

Figure 4.6 SEM images of aluminum samples at x500 magnifications (a) pure Al, (b) inoculated Al, (c) sample from bottom of furnace of inoculated Al at x500 magnifications and (d) sample from bottom of furnace of inoculated Al at x3.500 magnification.

Although the distribution rate of the intermetalic compound was low before inoculation, an increase on the rate was observed after the process. It was found that intermetallic compounds have the highest density in the bottom of liquid metal therefore reason is that plenty of intermetallic compound in aluminum are more dense than aluminum thereby as described in the previous chapters.

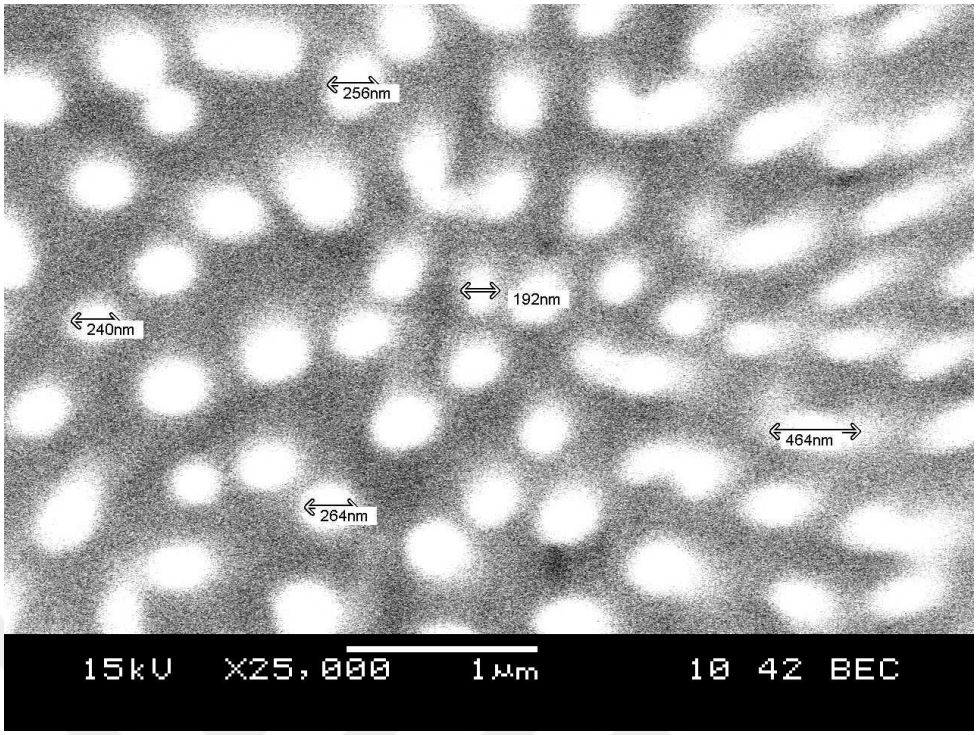

Figure 4.7 SEM analysis of Al-Fe-Si nanoparticles in inoculated Al sample from bottom of furnace at x25.000 magnification.

After the inoculation, the samples of the bottom of liquid metal include intermetallic compunds in various shapes and sizes. It is noted that the presence of the particles between 150-500 nm sizes showed by SEM analysis, as can be seen in Figure 4.7. These nanoparticles are Al-Fe-Si intermetallic compounds showing by EDS analysis (Figure 4.8).

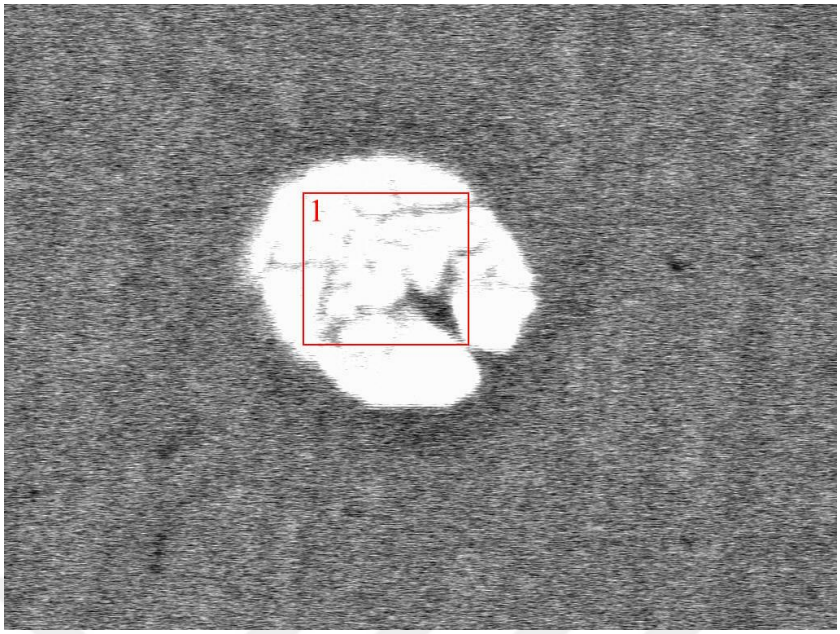

(a)

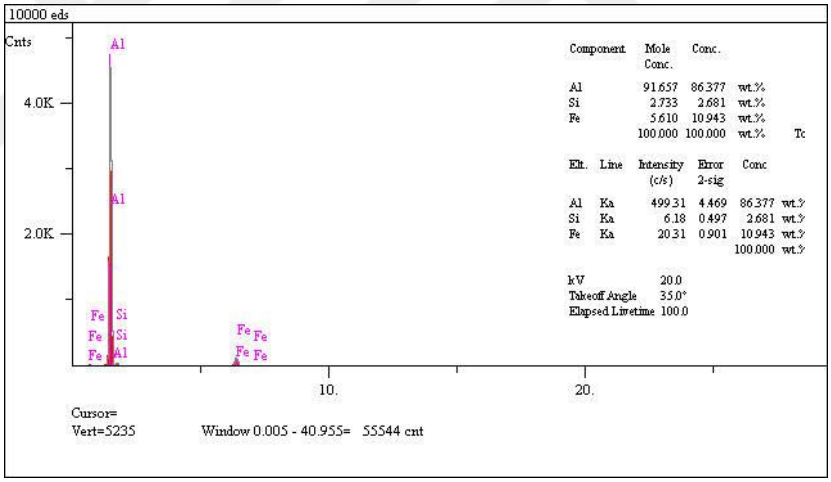

(b)

Figure 4.8 EDS analysis of pure Al (a) Al-Fe-Si intermetallic compound at 10.000x magnifiction and (b) EDS analysis result.

EDS analysis showed that the untidy structures in the pure aluminum sample are Al-Fe-Si intermetallic compounds.

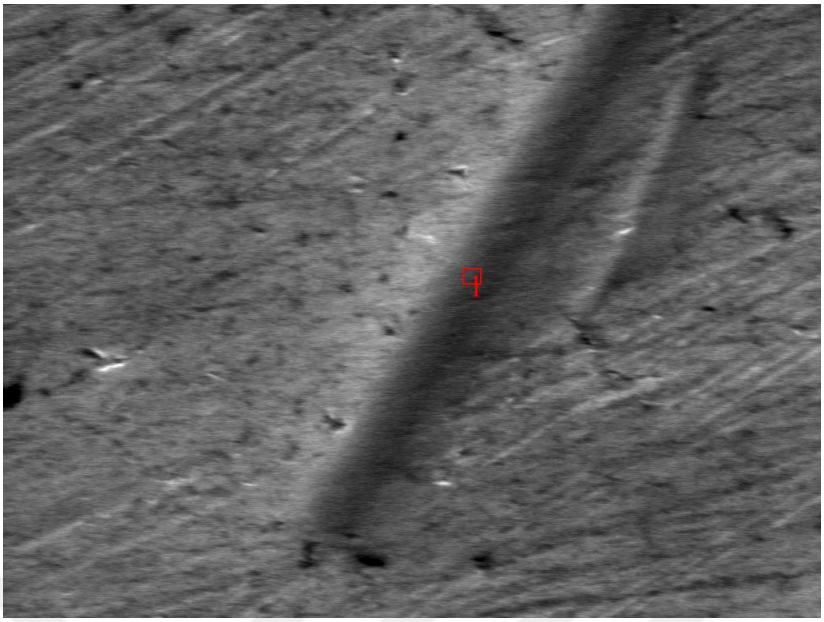

(a)

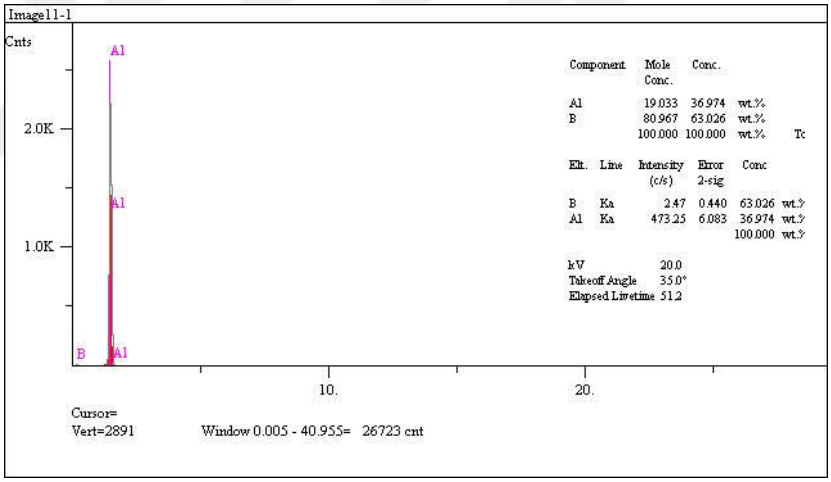

(b)

Figure 4.9 EDS analysis of inoculated aluminum (a) Al-B intermetallic rod at 10.000x magnifiction and (b) EDS analysis result.

The rod structure in the inoculated sample was determined by EDS analysis as Al-B intermetallic compound. It is determined that inoculation with Al-B master alloy is provided to increase formation of this structure.

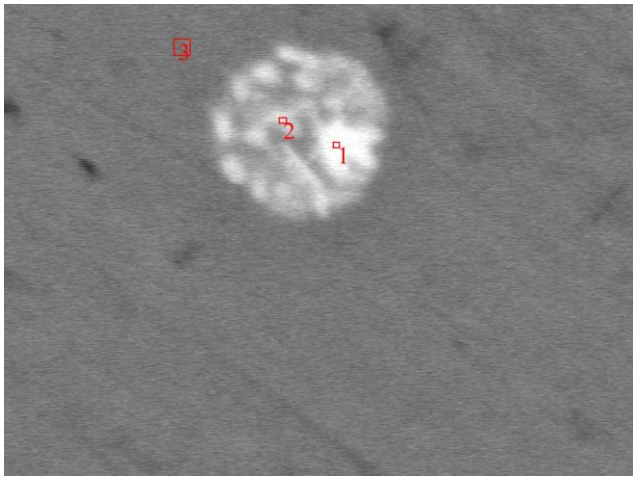

(a)

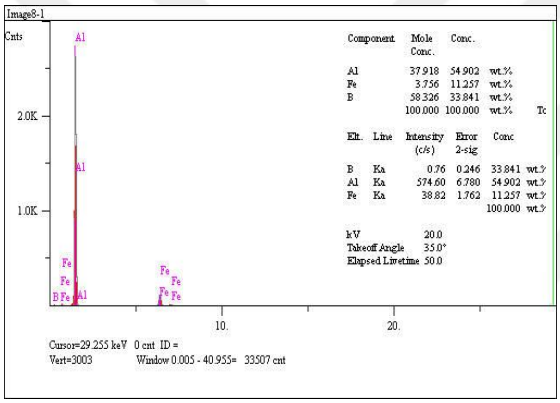

(b)

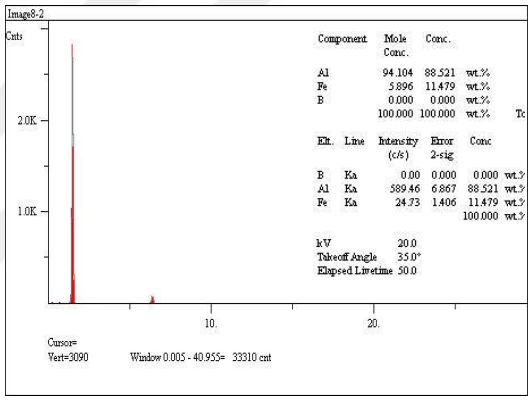

(c)

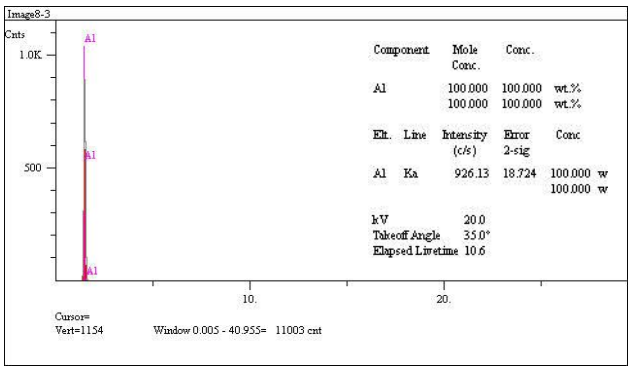

(d)

Figure 4.10 EDS analysis of inoculated Al sample from bottom of furnace (a) particule at 10.000x magnifiction, (b) EDS analysis result of Area 1, (c) EDS analysis result of Area 2 and (d) EDS analysis result of Area 1.

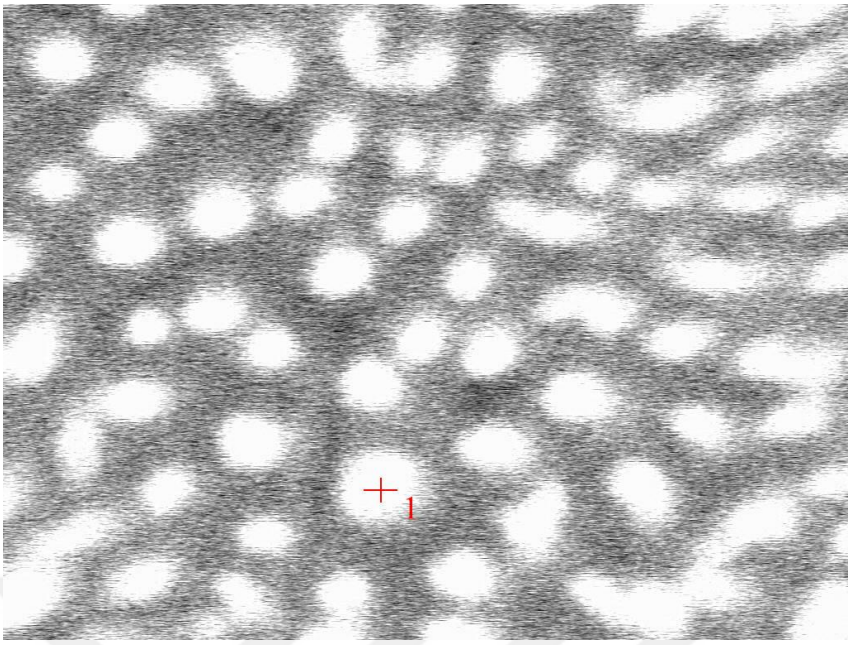

(a)

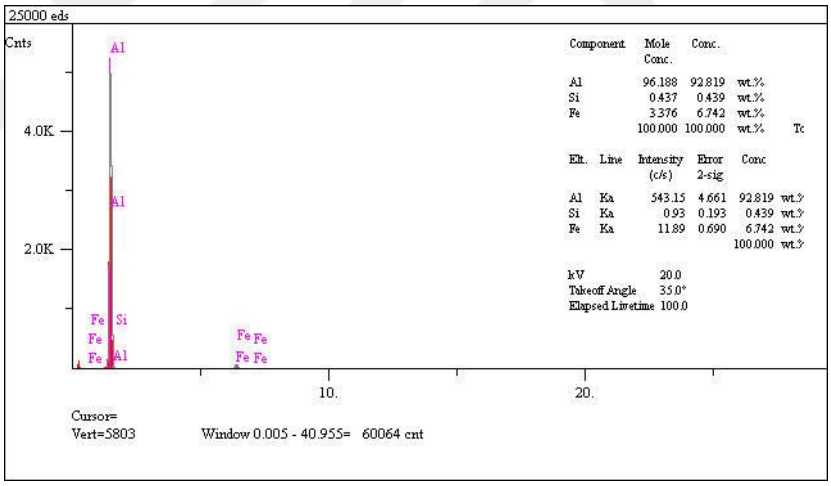

(b)

Figure 4.11 EDS analysis of inoculated Al sample from bottom of furnace (a) Al-Fe-Si nanoparticles at 25.000x magnifiction and (b) EDS analysis result.

Some structure was observed around Al-B particles formed Al-Fe and Al-Fe-Si intermetallic compounds when examinining many intermetallic compound samples from the bottom of liquid metal.

The appearence of these structures has been suggested that Al-B master alloy may have encouraged formation of intermetallic Al-Fe and Al-Fe-Si.

The maximum ability for soluble boron in aluminum is 0.022%. When the boron has been added to alloy for improving the electrical conductivity, its reacted with the impurity elements that in aluminum (V, Ti, Cr, Zr) and they are transformed to insoluble boride compounds (Wang, 2002). Reaction is begun in the first minutes of inoculation:

$$AlB_2 + M \longrightarrow AlMB_2 \quad (4.1)$$

$$AlB_{12} + 6M \longrightarrow Al(MB_2)_6 \quad (4.2)$$

Adding boron can removed transition metals such as Ti, V and Zr in aluminium. However, it can not be removed the other impurities such as Fe, Si and Cu as boride form (Dewan et al., 2011). They are separated from the matrix as $FeAl_3$ and $Al(Si,Ti)_2O(B)_3$. It has been reported that phase of $FeAl_3$ includes Ti in trace amount (Karabay, 2000).

Reaction of impurities with aluminum-boron compounds is fast and 70% of increase in electrical conductivity is achieved in the first stage and this increasing is continued for two hours. Heavy boride particules are occured as a results of the reaction and this boride particules are settled at the bottom of furnace. This settling is occured more when master alloys that includes AlB_{12} used. There is not enough studies to understand thermodynamics of boride formation inside alimunium (Khaliq, 2011).

4.5 Electrical Measurement

Before inoculation, after inoculation and heat treated samples conductivity, test results are shown in Table 4.2. According to tests, inoculation process has a positive effect on conductivity. Heat treatment at 400°C for 2 hours and 4 hours provide highest increase at electrical conductivity. Within more heat treatment time, Fe

diffusion possibility to rotor sticks increases. This is the reasons of choosing 2 hours of heat treatment.

Table 4.2 Electrical measurement of aluminum samples

Heat Treatment (°C)	Time (s)	Inoculant	IACS (%)
None	-	None	59
None	-	Al-3B	60.5
300	30	Al-3B	61.5
300	60	Al-3B	61.8
300	120	Al-3B	61.9
300	240	Al-3B	61.8
400	30	Al-3B	61.6
400	60	Al-3B	62
400	**120**	**Al-3B**	**62.2**
400	**240**	**Al-3B**	**62.3**
500	30	Al-3B	61.3
500	60	Al-3B	61.2
500	120	Al-3B	61.5
500	240	Al-3B	62

4.6 Magnetic Properties (VSM)

VSM results of samples with or without inoculation and heat treated are given in Figure 4.12. When hysteresis curves are analyzed, it is seen that pure aluminum reaches saturation point. However no saturation point was observed on inoculated aluminum's graphic. Sample with inoculation and heat treatment also does not reach saturation point and curve does not intersect with x axis. According to graphic it is fair to say that inoculation and heat treatment reduces magnetic properties of

aluminum. Additively aluminum used for this study is highly pure (99.7%). As a result of this magnetism is excessively lower. Therefore evaluations are based on comparative analysis.

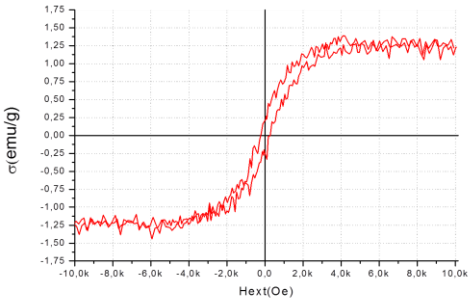

(a)

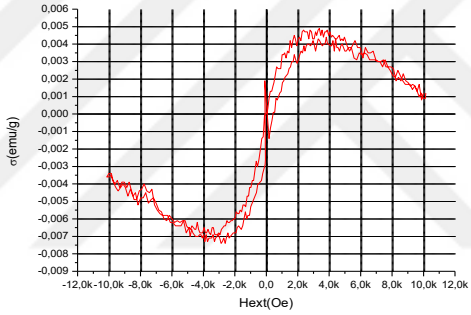

(b)

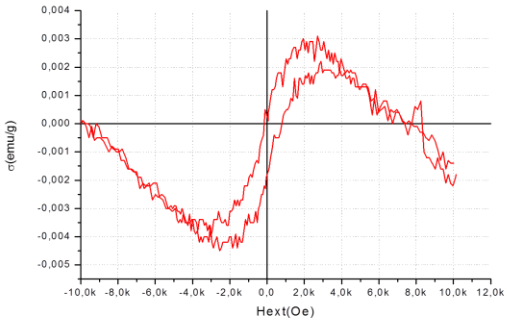

(c)

Figure 4.12 VSM analysis results of samples (a) pure aluminum, (b) inoculated aluminum and (c) inoculated and heat treated (at 400°C for 2 hours) aluminum.

4.7 Production of Prototype Motors and Performance Tests

For prototype motor production 100 kg pure Al was melted by using electrical furnace. After degassing and slag removal 300 g Al-3B master alloys was added. Liquid metal was waited around 2 hours then degassing and slag removal processes was repeated. After all rotor packages was placed to 50 ton vertical die casting machine and casting was performed. After casting, rotors were heat treated at 400°C for 2 hours within Ar atmosphere and water cooled (quenched). Efficiency differences between standard pure Al, master alloy Al (prototype) and heat treated master alloy Al shown in Table 4.3 and Table 4.4.

When rotor loss compared the biggest difference noticed on 90L/4 TYPE 1,5 kW motor group because of size of the motor. It is bigger than other motors thereby it contains more aluminum. As it is seen in Table 4.3, both master alloy and heat treated rotors's efficiency increased. After inoculation empurity elements segregated from solution and precipitated. This leads to increase of conductivity and efficiency. As a result of heat treatment metal oriented to (110) plane and prevented possible material defects thus conductivity and efficiency increased. Acquired motor performance test results verify studies which explained previous chapters.

Table 4.3 Performance tests of prototype motors

TYPE	VOLTAGE (V)	SPEED (RPM)	EFFICIENCY		
			Temp. Increase ΔT	**Indirect Efficiency**	Direct Efficiency
90L/2 TYPE 2,2 kW STANDARD	400	2852	52,5	**82,5**	83,3
90L/2 TYPE 2,2 kW PROTOTYPE	400	2854	54,3	**82,7**	82,7
90L/2 TYPE 2,2 kW PROTOTYPE - HEAT TREATMENT	400	2865	51,2	**83,4**	84,8
90S/2 TYPE 1,5 kW STANDARD	400	2874	40,2	**80,7**	83,6
90S/2 TYPE 1,5 kW PROTOTYPE	400	2877	38,1	**81,1**	84,4
90S/2 TYPE 1,5 kW PROTOTYPE - HEAT TREATMENT	400	2882	35,5	**81,8**	85,6
90L/4 TYPE 1,5 kW STANDARD	400	1395	49,7	**76,5**	78,5
90L/4 TYPE 1,5 kW PROTOTYPE	400	1411	49,7	**76,9**	79,7
90L/4 TYPE 1,5 kW PROTOTYPE - HEAT TREATMENT	400	1418	48,5	**78,5**	80,5

Table 4.4 Losses of prototype motors

TYPE	LOSSES					
	FRICTION AND WIND	IRON	STATOR	**ROTOR**	ADD. LOAD	TOTAL
90L/2 TYPE 2,2 kW STANDARD	41,6	104,8	137	**118,3**	61	462,7
90L/2 TYPE 2,2 kW PROTOTYPE	20	110	144	**117,8**	61	453,2
90L/2 TYPE 2,2 kW PROTOTYPE - HEAT TREATMENT	22,8	110,4	132,1	**106**	61	432,3
90S/2 TYPE 1,5 kW STANDARD	32	104,8	99,8	**66,9**	43	346,5
90S/2 TYPE 1,5 kW PROTOTYPE	41,9	90	95	**65,3**	43	335,2
90S/2 TYPE 1,5 kW PROTOTYPE - HEAT TREATMENT	35,6	85,8	92,7	**62**	43	319,1
90L/4 TYPE 1,5 kW STANDARD	14,3	101,9	172,9	**114,7**	46	449,8
90L/4 TYPE 1,5 kW PROTOTYPE	15,1	101,6	173,6	**95,4**	46	453,7
90L/4 TYPE 1,5 kW PROTOTYPE - HEAT TREATMENT	14	90	170	**90**	46	410

CHAPTER FIVE
CONCLUSION AND FUTURE PLANS

5.1 General Results

After all analyzes, as a result of inoculation between 99.7% Al and Al-B master alloy amount of impurity decreased and with this decreasing conductivity has been raised.

XRD analyzes results (Figure 4.2) established pure Al. All analyze results lead conclusion of inoculation with 3% Boron Al-B master alloy and heat treatment cause more conductivity than pure aluminum. Reasons of this increase are, impurity elements pass slag and remain at structure as boride such as TiB, VB_2, CrB and intermetalic compound such as Al-Fe-Si and Al-Fe. On the other side, heat treatment was oriented to (110) plane and prevented possible material defects thus conductivity and efficiency increased.

The summarized results can be sum up as follows:

- As a result of inoculation with Al-3B master alloys, the purity of aluminum are increased, because of impurity elements pass to slag and remain at structure as boride such as TiB, VB_2, CrB and intermetalic compound such as Al-Fe-Si and Al-Fe.

- Some structure was observed around Al-B particles formed Al-Fe and Al-Fe-Si intermetallic compounds when examinining many intermetallic compound samples from the bottom of liquid metal. The appearence of these structures has been suggested that Al-B master alloy may have encouraged formation of intermetallic Al-Fe and Al-Fe-Si.

- Heat treatment at 400°C 2 hours and 4 hours provide highest increase at electrical conductivity. As a result of heat treatment was oriented to (110) plane and prevented possible material defects thus conductivity and efficiency increased.

In this research, both inoculation with Al-3B master alloy and heat treatment were decreased rotor losses. For this reason, motor efficiency was increased.

5.2 Future Plans

There are some suggestions and research subjects that should be investigated for future works on the subject of this thesis. Higher rates of inoculant usage may be attempted to eliminate impurities in the aluminum. After heat treatment, applied in air or furnace cooling for the rotors which used in large motor types to prevent damage due to thermal shock.

REFERENCES

Aksöz, S., Ocak, Y., Maraşlı, N., Çadirli, E., Kaya, H., & Böyük, U. (2010). Dependency of the thermal and electrical conductivity on the temperature and composition of Cu in the Al based Al-Cu alloys. *Experimental Thermal and Fluid Science, 34* (8), 1507-1516.

ASM International. (1990). *ASM metals handbook volume 02: Properties and selection nonferrous alloys and special purpose materials* (492). Cleveland: American Society of Metals.

Buschow, K. H. J., & de Boer, F. R. (2004). *Physics of magnetism and magnetic materials* (1st Ed.). New York: Kluwer Academic Publishers.

Callister, W. D., & Rethwisch, D. G. (2010). *Materials science and engineering: An introduction* (8th Ed.). New York: John Wiley & Sons, Inc.

Cooper, P. S., & Kearns, M. A. (1996). Removal of transition metal impurities in aluminum melts by boron additives. *Material Science Forum, 217*, 141-146.

Crist, B.V. (2011). *X-rayphotoelectron spectroscopy*. Retrieved August 21, 2015, from http://en.wikipedia.org/wiki/X-ray_photoelectron_spectroscopy.

Deppisch, C., Liu, G., Shang, J. K., & Economy, J. (1997). Processing and mechanical properties of AlB_2 flake reinforced Al-alloy composites. *Material Science and Engineering, A225,* 153–161.

Dewan, M. A., Rhamdhani, M. A., Mitchell, J. B., Davidson, C. J., Brooks, G. A., Easton M., et al. (2011). Control and removal of impurities from Al melts: A review. *Materials Science Forum , 693*, 149-160.

Duschanek, H., & Rogl, P. (1994). The Al-B (aluminum-boron) system. *Journal of Phase Equilibria, 15* (5), 543–552.

Feng, C., Liu, Z., Ning, A., Liu, Y., & Zeng, S. (2006). Retrogression and re-aging treatment of Al-9.99%Zn-1.72%Cu-2.5%Mg-0.13%Zr aluminum alloy. *Transactions of Nonferrous Metals Society of China, 16* (5), 1163-1170.

Fjellsted, J., Jarfors A., & Svendsen L. (1999). Experimental analysis of the intermediary phases AlB2, AlB12and TiB2 in the Al–B and Al–Ti–B systems. *Journal of Alloys and Compounds, 283* (1-2), 192–197.

Giardini, A. A., Kohn, J. A., Toman, L., & Eckart, D.W. (1960). Vector hardness properties of boron and aluminum borides. In J. A. Kohn, (Ed.), W. F. Nye, (Ed.), G. K. Gaule, (Ed.). *Boron synthesis, structure and properties* (1st Ed.) (140-158). New York: Plenum Press.

Giridhar, P., Weidenfeller, B., Zein El Abedin, S., & Endres, F. (2014). Electrodeposition of iron and iron–aluminium alloys in an ionic liquid and their magnetic properties. *Physical Chemistry Chemical Physics, 16*, 9317-9326.

Gupta, J. B. (2010). *Theory & performance of electrical machines* (14th Ed.). New Delhi: S.K. Kataria & Sons.

Hofmann, W., & Janiche, Z. (1936). The structure of aluminum boride, AlB2. *Zeitschrift für Physikalische Chemie, 31*, 214–222.

Karabay, S., & Uzman, I. (2005). Inoculation of transistion elements by addition of AlB2 and AlB12 to decrease detrimental effect on the conductivity of 99.6 % aluminium in CCL for manufacturing of conductor. *Journal of Material Processing Technology, 160* (2), 174-182.

Karabay, S. (2006). Modification of AA-6201 alloy for manufacturing of high conductivity and extra high conductivity wires with property of high tensile stres after artificial aging heat treatment for all-aluminium alloy conductors. *Materials and Design*, *27* (10), 821-832.

Karabay, S. (2008). Influence of AlB2 compound on elimination of incoherent precipitation in artificial aging of wires drawn from redraw rod extruded from billets cast of alloy AA-6101 by vertical direct chill casting. Materials and Design, 29 (7), 1364-1375.

Karabay, S. (2010). *Yüksek Ti, V ve Cr muhtevalı %99.6 - %99.7 saflıkta alüminyum dökümlerin sürekli döküm hatlarında haddeleme öncesi elektriksel iletkenlik özelliklerinin iyileştirilmesi ve endüstride iletken yapımında kullanılabilirliklerinin araştırılması*. Ph.D. Thesis, Kocaeli University, Kocaeli.

Khaliq, A., Rhamdhani, M. A., Brooks, G. A., & Grandfield, J. (2011). Thermodynamic analysis of Ti, Zr, V and Cr impurities in aluminum melt. In S. J. Lindsay, (Ed.). *Light metals* (1st Ed.) (751-756). New Jersey: John Wiley & Sons, Inc.

Kirihara, K., Nagata, T., & Kimura K. (2002). Thermoelectric properties of AlPdRe icoshedral alloys. *Journal of Alloys and Compounds, 342*, 469-472.

Kutner, F. (1981). *Aluminum-monograph, aluminum conductor materials* (1st Ed.) (15-27). Düsseldorf: GmbH: Aluminum-Verlag.

Moulson, A. J., & Herbert, J. M. (2003). *Electroceramics: Materials, properties, applications* (2nd Ed.). Chichester: John Wiley & Sons, Inc.

Prabhu, K. N., & Ravishankar, B. N. (2003). Effect of modification melt treatment on casting/chil interfacial heat transfer and electrical conductivity of Al-13%Si alloy. *Materials Science and Engineering: A, 360* (1-2), 293-298.

Sabirov, I., Murashkin, M. Y., & Valiev, R. Z. (2013). Nanostructured aluminium alloys produced by severe plastic deformation: New horizons in development. *Materials Science and Engineering: A, 560*, 1-24.

Shimadzu (2015). *Principle of optical emission spectrometry*. Retrieved August 21, 2015, from http://www.shimadzu.com/an/elemental/oes/oes.html.

Sigmascope (2015). *Sigmascope SMP 10*. Retrieved August 21, 2015, from http://www.acutech.gr/media/pdf/de_sigmascope_en.pdf.

Slemon, G. R. (1966). *Magnetoelectric devices: Transducers, transformers, and machines* (1st Ed.) (384-389). New York: John Wiley and Sons, Inc.

Smontara, A., Smiljanic, I., Blusic, A., Grushko, B., Balanetskyy, S., Jaglicic, S., et al. (2008). Complex ε-phases in the Al-Pd-transistion-metal systems: Towards a combination of an electrical conductor with a thermal insulator. *Journal of Alloys and Compounds, 450*, 92-102.

Spaldin, N. A. (2010). *Magnetic materials fundamentals and applications* (2nd Ed.). New York: Cambridge University Press.

Stiller, W., & Ingenlath, T. (1984). Industrial boron treatment of aluminium conductor alloys and its influence on grain refinement and electrical conductivity. *Aluminium (English Edition), 60*, 577–580.

U.S. Department of Energy. (2008). *Improving motor and drive system performance: A sourcebook for industry*.

Ueda Y., Hashimoto E., Tamura H., & Kino, T. (1995). Anisotropy of Electrical Resistivity in High-Purity Aluminium Single Crystals. *Journal de Physique IV, 5* (C7), 287-292.

Vandaele, K. (2011). *YBa2Cu3O7 coatings based on trifluoro-acetic acid precursors*. University of Cambridge, M.Sc Thesis, United Kingdom.

Volt Electric Motors Company (2013). *Volt Electric Motors Catalog*.

Wang, G., Liu, S., Li, C., & Gao, Q. (2002)." Reaction of boron to transition metal impurities and its effect on conductivity of aluminum" *Transactions of Nonferrous Metals Society of China, 12* (6), 1112-1116.

Wang, X. (2005). The formation of AlB_2 in an Al-B master alloy. *Journal of Alloys and Compounds 403*, 283–287.

Willey, L. A. (1967). In K.R. Van Horn, (Ed.). *Aluminium vol. 1: Properties, Physical Metallurgy and Phase Diagrams* (174). Cleveland: American Society of Metals.

Zupanic, F., Spaic, S., & Krizman, A. (1998). Contribution to ternary system Al-Ti-B Part 2: Study of alloys in Al-AlB(2)-TiB2 triangle. *Material Science and Technology, 14* (12), 1203–1212.